Literature study for thesis project

Modelling and simulating three phases of steel:
austenite, ferrite and cementite

Thijs Verbeek

May 2, 2017

Contents

Chapter 1

Introduction

Steel is an important material used in the construction of many different things. Steel is originally an alloy of iron (Fe) and a small amount of carbon (C), normally up to about 2.1% of the total weight. To improve certain properties of steel other alloying elements such as manganese, nickel, chromium, molybdenum, boron, titanium, vanadium, tungsten, cobalt, and niobium can be added. The iron atoms in steel are structured in two different crystalline forms, face centered cubic (FCC) and body centered cubic (BCC). These two crystalline forms can contain different quantity of carbon, influencing its hardness, ductility and tensile strength. FCC structured steel is called austenite (γ) and BCC structured steel is called ferrite (α). In the transition from austenite to ferrite by cooling, cementite (θ) can also be present. Cementite is a stoichiometric compound with formula Fe_3C, meaning 6.67% of its weight is carbon and 93.3% is iron. In the making of steel, cooling is mostly done by quenching. This is the rapid cooling of the steel in order to preserve properties of the FCC-structured steel.

The transition from austenite to ferrite can modelled by a so-called Stefan problem. It describes the diffusion of carbon in the different phases and the movement of its interfaces. When numerically solving the Stefan problem, keeping track of the interfaces can be complicated, especially when there are multiple phases connected. In this project we model the mechanism of ferrite growth just after nucleating at the interface between austenite and cementite (see Figure 1.1). The goal of this thesis project is to make a two dimensional implementation using the level-set method. This literature study is used as an introduction to the model itself and the physics of it. Some choices regarding the numerical implementation and the physical parameters will be based upon the results from the one dimensional model.

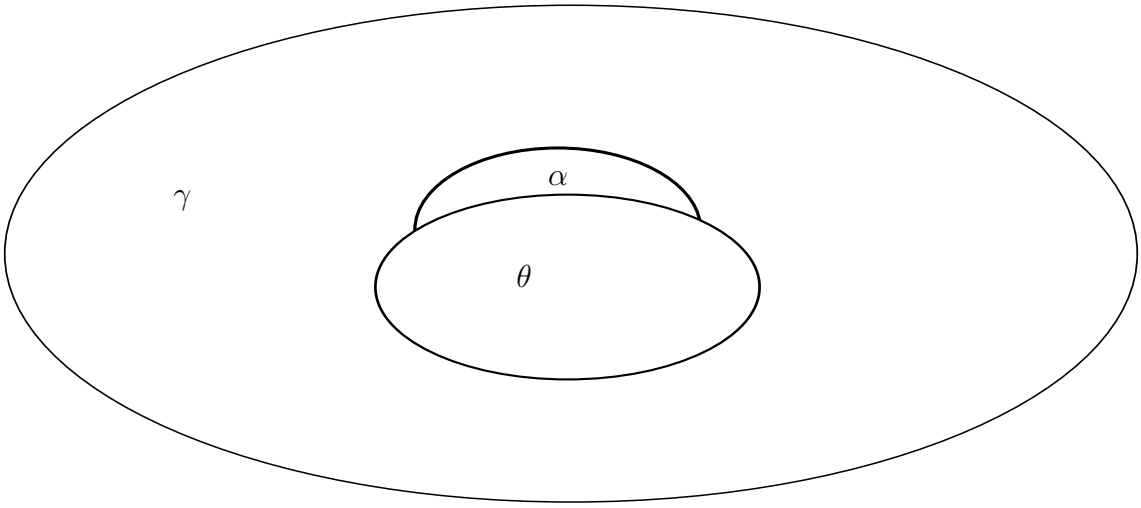

Figure 1.1: Sketch of the nucleation of ferrite (α) on the interface of austenite (γ) and cementite (θ).

First in chapter 2 the Stefan problem for the diffusion of carbon is defined and different possible boundary conditions are treated. Then to numerically capture the movement of the interfaces, the level-set method is shown and also several other boundary moving methods are briefly looked at in chapter 3. In chapter 4 the differential equation of the Stefan problem is discretised in space using Galerking Finite Element Method and in time with a first -and a second order time discretisation technique. The physical parameters of the model are given in chapter 5. Then in chapter 6 the results of a 1D implementation are shown and in chapter 7 discussed. Also in chapter 7 a brief summary of the future research is given as guideline for the rest of this master thesis research.

Chapter 2

Model

The model presented here is based on the Stefan problem. The model described in den Ouden's phd thesis [1] models a two-phase domain with interaction between a matrix and a precipitate, austenite (γ) and cementite (θ) respectively. In this research a second matrix phase is introduced, namely the phase ferrite (α). It is assumed that the ferrite domain just nucleated on the interface between austenite and cementite. It is on this interface that the most free energy is available for nucleation. Such a nucleation occurs when temperature is lowered from a temperature where there is austenite and cementite equilibrium to a temperature where there is ferrite and cementite equilibrium (Figure 2.1). Free energy on the interface will only build up for temperatures below the austenite/cementite equilibrium line, thus only under $A_1 = 1000$ K, which is called the eutectoid temperature. For this model we assume ferrite to have nucleated at 995 K. Over time all austenite will dissolve and ferrite will grow. This dispersion/growth is controlled by the diffusion in the matrices and the behaviour of the three interfaces between austenite and ferrite, austenite and cementite and ferrite and cementite. Each of these interfaces describe different reactions between the phases and need a corresponding physical boundary condition. The partial differential equation of the Stefan problem described in the phase domains, prescribing the concentration of carbon, is the following:

$$\begin{cases} \frac{\partial c_\gamma}{\partial t}(\mathbf{x},t) &=& \nabla \cdot (D_\gamma(\mathbf{x},t)\nabla c_\gamma(\mathbf{x},t)) & \text{, for } \mathbf{x} \in \Omega_\gamma(t), t > t_0, \\ \frac{\partial c_\alpha}{\partial t}(\mathbf{x},t) &=& \nabla \cdot (D_\alpha(\mathbf{x},t)\nabla c_\alpha(\mathbf{x},t)) & \text{, for } \mathbf{x} \in \Omega_\alpha(t), t > t_0, \\ c_\theta(\mathbf{x},t) &=& c_\theta & \text{, for } \mathbf{x} \in \Omega_\theta(t), t > t_0, \\ c(\mathbf{x},t) &=& c_0 & \text{, for } \mathbf{x} \in \Omega, t = t_0, \end{cases} \tag{2.1}$$

where $\Omega_\gamma(t)$ and $\Omega_\alpha(t)$ are the diffusion domain of matrix austenite and ferrite phases respectively. $\Omega_\theta(t)$ is the precipitate domain of cementite, where the concentration

of carbon is assumed constant. This assumption is made because the carbon atoms in cementite are able to diffuse almost instantly compared to austenite/cementite and thus believed to have the same concentration level over its domain. c_0 is the initial solution at $t = t_0$.

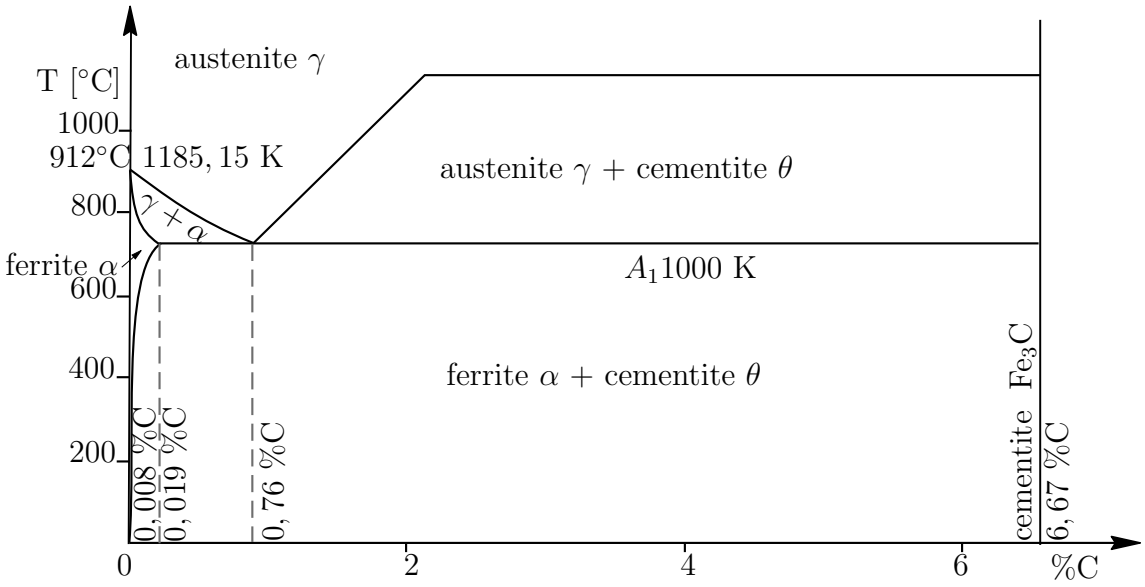

Figure 2.1: Phase diagram with the lines representing the equilibrium wt % lines.

The three interfaces between the three domains will have their own boundary conditions, which are considered in the following section. The interfaces between austenite/ferrite, austenite/cementite and ferrite/cementite will be denoted as $\Gamma^{\gamma\alpha}(t), \Gamma^{\gamma\theta}(t)$ and $\Gamma^{\alpha\theta}(t)$ respectively. The order in which the two symbols are notated will also define the normal vectors' direction on these interfaces. Meaning the normal vector on $\Gamma^{\gamma\alpha}(t)$ points from $\Omega_\gamma(t)$ to $\Omega_\alpha(t)$ and $\mathbf{n}^{\gamma\alpha} = -\mathbf{n}^{\alpha\gamma}$. The total domain is the union of $\Omega_\gamma(t), \Omega_\alpha(t), \Omega_\theta(t)$, the interfaces $\Gamma^{\gamma\alpha}(t), \Gamma^{\gamma\theta}(t), \Gamma^{\alpha\theta}(t)$ and the outer boundary $\partial\Omega$. It is defined as $\Omega(t) = \overline{\Omega_\gamma}(t) \cup \overline{\Omega_\alpha}(t) \cup \overline{\Omega_\theta}(t)$, where $\overline{\Omega}$ is the domain including its boundaries.

2.1 Boundary conditions

2.1.1 Outer boundary

At the outer boundary $\partial\Omega(t)$ no carbon atoms can get in or out of the system. Which means:

$$\frac{\partial c}{\partial n}(\mathbf{x}, t) = 0, \text{ for } \mathbf{x} \in \partial\Omega(t). \tag{2.2}$$

This also means the shape of $\Omega(t)$ does not change, which implies $\Omega(t) = \Omega$ and $\partial\Omega(t) = \partial\Omega$. A homogeneous Neumann boundary condition is practical and realistic, as it will imply no change in mass over Ω. A periodical boundary condition could also be used, which also results in mass conservation.

2.1.2 Stefan condition

An important condition on the model is the conservation of mass. As the flux over the outer boundary is zero, we know that the total change in mass over Ω should also be zero. If we then look individually per domain, the changes in mass should add up to zero, meaning:

$$\frac{dM}{dt}(t) = \frac{d\left(M_\gamma(t) + M_\alpha(t) + M_\theta(t)\right)}{dt} = 0. \tag{2.3}$$

This condition is commonly known as the Stefan condition.
For the diffusive phase $\Omega_\gamma(t)$:

$$\frac{dM_\gamma}{dt}(t) = \frac{d}{dt}\int_{\Omega_\gamma(t)} c_\gamma(\mathbf{x}, t)d\Omega =$$
$$\int_{\Gamma^{\gamma\alpha}(t)} D_\gamma(\mathbf{x}, t)\frac{\partial c_\gamma}{\partial n}(\mathbf{x}, t)d\Gamma + \int_{\Gamma^{\gamma\theta}(t)} D_\gamma(\mathbf{x}, t)\frac{\partial c_\gamma}{\partial n}(\mathbf{x}, t)d\Gamma +$$
$$\int_{\Gamma^{\gamma\alpha}(t)} c_\gamma(\mathbf{x}, t)v_n^{\gamma\alpha}(\mathbf{x}, t)d\Gamma + \int_{\Gamma^{\gamma\theta}(t)} c_\gamma(\mathbf{x}, t)v_n^{\gamma\theta}(\mathbf{x}, t)d\Gamma.$$

Here we used Reynold's transport theorem, the product rule and Gauss' theorem. The homogeneous Neumann boundary condition on $\partial\Omega$ cancels this term. $c_\gamma(\mathbf{x}, t)$ is the concentration of carbon in $\Omega_\gamma(t)$ and $v_n^{\gamma\alpha}(\mathbf{x}, t), v_n^{\gamma\theta}(\mathbf{x}, t)$ are the velocities of the interfaces $\Gamma^{\gamma\alpha}(t), \Gamma^{\gamma\theta}(t)$ respectively.

A similar equation will hold for $\Omega_\alpha(t)$:

$$\frac{dM_\alpha}{dt}(t) = \int_{\Gamma^{\gamma\alpha}(t)} -D_\alpha(\mathbf{x},t)\frac{\partial c_\alpha}{\partial n}(\mathbf{x},t)d\Gamma + \int_{\Gamma^{\alpha\theta}(t)} D_\alpha(\mathbf{x},t)\frac{\partial c_\alpha}{\partial n}(\mathbf{x},t)d\Gamma + \int_{\Gamma^{\gamma\alpha}(t)} -c_\alpha(\mathbf{x},t)v_n^{\gamma\alpha}(\mathbf{x},t)d\Gamma + \int_{\Gamma^{\alpha\theta}(t)} c_\alpha(\mathbf{x},t)v_n^{\alpha\theta}(\mathbf{x},t)d\Gamma.$$

The change in mass of the precipitate θ:

$$\frac{dM_\theta}{dt}(t) = \frac{d}{dt}\int_{\Omega_\theta(t)} c_\theta(\mathbf{x},t)d\Omega = \int_{\Gamma^{\alpha\theta}(t)} -c_\theta v_n^{\alpha\theta}(\mathbf{x},t)d\Gamma + \int_{\Gamma^{\gamma\theta}(t)} -c_\theta v_n^{\gamma\theta}(\mathbf{x},t)d\Gamma.$$

Adding all these together we get:

$$\frac{dM}{dt}(t) = \int_{\Gamma^{\gamma\theta}(t)} \left(c_\gamma(\mathbf{x},t) - c_\theta\right) v_n^{\gamma\theta}(\mathbf{x},t) + D_\gamma(\mathbf{x},t)\frac{\partial c_\gamma}{\partial n}(\mathbf{x},t)d\Gamma + \int_{\Gamma^{\alpha\theta}(t)} \left(c_\alpha(\mathbf{x},t) - c_\theta\right) v_n^{\alpha\theta}(\mathbf{x},t) + D_\alpha(\mathbf{x},t)\frac{\partial c_\alpha}{\partial n}(\mathbf{x},t)d\Gamma + \int_{\Gamma^{\gamma\alpha}(t)} \left(c_\gamma(\mathbf{x},t) - c_\alpha(\mathbf{x},t)\right) v_n^{\gamma\alpha}(\mathbf{x},t) + D_\gamma(\mathbf{x},t)\frac{\partial c_\gamma}{\partial n}(\mathbf{x},t) - D_\alpha(\mathbf{x},t)\frac{\partial c_\alpha}{\partial n}(\mathbf{x},t)d\Gamma = 0.$$

As these interfaces can still be chosen arbitrarily, the change in mass $M(t)$ can only be zero as each of the three individual interface integrals are zero. Meaning:

$$\int_{\Gamma^{\gamma\theta}(t)} \left(c_\gamma(\mathbf{x},t) - c_\theta\right) v_n^{\gamma\theta}(\mathbf{x},t) + D_\gamma(\mathbf{x},t)\frac{\partial c_\gamma}{\partial n}(\mathbf{x},t)d\Gamma = 0,$$

$$\int_{\Gamma^{\alpha\theta}(t)} \left(c_\alpha(\mathbf{x},t) - c_\theta\right) v_n^{\alpha\theta}(\mathbf{x},t) + D_\alpha(\mathbf{x},t)\frac{\partial c_\alpha}{\partial n}(\mathbf{x},t)d\Gamma = 0,$$

$$\int_{\Gamma^{\gamma\alpha}(t)} \left(c_\gamma(\mathbf{x},t) - c_\alpha(\mathbf{x},t)\right) v_n^{\gamma\alpha}(\mathbf{x},t) + D_\gamma(\mathbf{x},t)\frac{\partial c_\gamma}{\partial n}(\mathbf{x},t) - D_\alpha(\mathbf{x},t)\frac{\partial c_\alpha}{\partial n}(\mathbf{x},t)d\Gamma = 0.$$

Which in turn implies that the terms inside the integrals should be zero, giving the Stefan conditions:

$$(c_\gamma(\mathbf{x},t) - c_\theta)\, v_n^{\gamma\theta}(\mathbf{x},t) + D_\gamma(\mathbf{x},t)\frac{\partial c_\gamma}{\partial n}(\mathbf{x},t) = 0, \quad \text{for } \mathbf{x} \in \Gamma^{\gamma\theta}(t), t > t_0. \tag{2.4}$$

$$(c_\alpha(\mathbf{x},t) - c_\theta)\, v_n^{\alpha\theta}(\mathbf{x},t) + D_\alpha(\mathbf{x},t)\frac{\partial c_\alpha}{\partial n}(\mathbf{x},t) = 0, \quad \text{for } \mathbf{x} \in \Gamma^{\alpha\theta}(t), t > t_0. \tag{2.5}$$

$$(c_\gamma(\mathbf{x},t) - c_\alpha(\mathbf{x},t))\, v_n^{\gamma\alpha}(\mathbf{x},t) + D_\gamma(\mathbf{x},t)\frac{\partial c_\gamma}{\partial n}(\mathbf{x},t) - D_\alpha(\mathbf{x},t)\frac{\partial c_\alpha}{\partial n}(\mathbf{x},t) = 0, \quad \text{for } \mathbf{x} \in \Gamma^{\gamma\alpha}(t), t > t_0. \tag{2.6}$$

Note that there are two unknowns for (2.4), $c_\gamma(\mathbf{x},t)$ and $v_n^{\gamma\theta}(\mathbf{x},t)$. Also two for (2.5), $c_\alpha(\mathbf{x},t)$ and $v_n^{\alpha\theta}(\mathbf{x},t)$ and three for (2.6), $c_\gamma(\mathbf{x},t), c_\alpha(\mathbf{x},t)$ and $v_n^{\gamma\alpha}(\mathbf{x},t)$. Meaning that there is one more condition required for (2.4) and (2.5) and two more conditions for (2.6) to suffice the model. In the rest of this chapter several boundary conditions are considered.

2.1.3 Matrix-precipitate boundary

There are three physical phenomena active [1] at the matrix-precipitate interfaces $\Gamma^{\gamma\theta}(t), \Gamma^{\alpha\theta}(t)$:

1. Atoms coming lose from the lattice structure of the precipitate phase.

2. Moving atoms from within the precipitate going into the matrix.

3. Long distance diffusion of atoms in the matrix.

At the matrix-precipitate boundary many models assume that the diffusive behaviour limits the growth/dissolution of the model and neglects the possible influence of the first two reaction-like phenomenon given above. In the work of Vermolen [2] it has been shown that these interface reactions can have a significant influence on the dissolution for a plate-like precipitate. When neglecting these effects a simple Dirichlet boundary can be chosen to complement the Stefan condition for the matrix-precipitate interfaces. Physically this means the concentration is at local equilibrium on the interfaces at all time.

Local equilibrium

Assuming that the concentrations $c_\gamma(\mathbf{x},t), c_\alpha(\mathbf{x},t)$ are known at the interfaces $\Gamma^{\gamma\theta}(t)$, $\Gamma^{\alpha\theta}(t)$ gives

$$c_k(\mathbf{x},t) = c_{k\theta}^{\text{sol}}(\mathbf{x},t), \text{for } \mathbf{x} \in \Gamma^{k\theta}(t), t > t_0, k = \gamma, \alpha, \tag{2.7}$$

where $c_{k\theta}^{\text{sol}}(\mathbf{x},t)$ is called the solubility, or the local equilibrium concentration, of the phase k on θ. An addition to this condition can be adding curvatures effects to the solubility at the interfaces of the domains. This effect is known as the Gibbs-Thomson effect [3] and is described as:

$$c_{k\theta}^{\text{sol}}(\mathbf{x},t) = c_{k\theta}^{\infty}(t) \exp\left\{ \frac{E_{k\theta} V_m}{R_g T(t)} \kappa(\mathbf{x},t) \right\}, \text{for } \mathbf{x} \in \Gamma^{k\theta}(t), t > t_0, k = \gamma, \alpha, \tag{2.8}$$

where $c_{k\theta}^{\infty}(t)$ is the equilibrium concentration with no space dependency, of phase $k = \gamma, \alpha$ with respect to θ. $E_{k\theta}$ is the interface energy, V_m the molar volume of θ, R_g the gas constant, $T(t)$ the temperature and $\kappa(\mathbf{x},t)$ the sum of the principle curvatures of $\Gamma^{k\theta}(t)$. This curvature effect will cause the precipitate to grow/dissolve to a formation where overall surface tension is lowest, i.e. the total energy of the system will be minimized [4].

Reaction boundary condition

The first and second phenomena given earlier across the interface is assumed to be a first-order reaction in terms of its flux:

$$J_r^{k\theta}(\mathbf{x},t) = -K^{k\theta}(\mathbf{x},t) \left(c_{k\theta}^{\text{sol}}(\mathbf{x},t) - c_k(\mathbf{x},t) \right), \text{ for } \mathbf{x} \in \Gamma^{k\theta}(t), t > t_0, k = \gamma, \alpha. \tag{2.9}$$

Here $K^{k\theta}(\mathbf{x},t)$ is the interface-reaction speed and $c_{k\theta}^{\text{sol}}(\mathbf{x},t)$ the solubility, which can also be extended with the Gibbs-Thomson effect (2.8).
The fluxes within the diffusive domains $\Omega_\gamma(t), \Omega_\alpha(t)$ at the interfaces consist of two parts. The flux $J_m^{k\theta}(\mathbf{x},t)$ generated by movement of the interface

$$J_m^{k\theta}(\mathbf{x},t) = -c_k(\mathbf{x},t) v_n^{k\theta}(\mathbf{x},t), \text{ for } \mathbf{x} \in \Gamma^{k\theta}(t), t > t_0, k = \gamma, \alpha \tag{2.10}$$

and the diffusive flux

$$J_d^{k\theta}(\mathbf{x},t) = -D_k(\mathbf{x},t) \frac{\partial c_k}{\partial n}(\mathbf{x},t), \text{ for } \mathbf{x} \in \Gamma^{k\theta}(t), t > t_0, k = \gamma, \alpha. \tag{2.11}$$

Requiring the net flux to be zero, gives the flux boundary condition:

$$-K^{k\theta}(\mathbf{x},t) \left(c_{k\theta}^{\text{sol}}(\mathbf{x},t) - c_k(\mathbf{x},t) \right) = -c_k(\mathbf{x},t) v_n^{k\theta}(\mathbf{x},t) - D_k(\mathbf{x},t) \frac{\partial c_k}{\partial n}(\mathbf{x},t), \tag{2.12}$$
$$\text{for } \mathbf{x} \in \Gamma^{k\theta}(t), t > t_0, k = \gamma, \alpha.$$

Together with the Stefan condition (2.4), (2.5) we get

$$v_n^{k\theta}(\mathbf{x},t) = \frac{K^{k\theta}(\mathbf{x},t)}{c_\theta}\left(c_{k\theta}^{\mathrm{sol}}(\mathbf{x},t) - c_k(\mathbf{x},t)\right), \text{ for } \mathbf{x} \in \Gamma^{k\theta}(t), t > t_0, k = \gamma, \alpha \quad (2.13)$$

and

$$D_k(\mathbf{x},t)\frac{\partial c_k}{\partial n}(\mathbf{x},t) = \frac{K^{k\theta}(\mathbf{x},t)}{c_\theta}\left(c_\theta - c_k(\mathbf{x},t)\right)\left(c_{k\theta}^{\mathrm{sol}}(\mathbf{x},t) - c_k(\mathbf{x},t)\right), \quad (2.14)$$
$$\text{for } \mathbf{x} \in \Gamma^{k\theta}(t), t > t_0, k = \gamma, \alpha.$$

Note that from this we can see that

$$c_k(\mathbf{x},t) = c_{k\theta}^{\mathrm{sol}}(\mathbf{x},t) - \frac{c_\theta}{K^{k\theta}(\mathbf{x},t)} v_n^{k\theta}(\mathbf{x},t), \text{for } \mathbf{x} \in \Gamma^{k\theta}(t), t > t_0, k = \gamma, \alpha. \quad (2.15)$$

This implies that for large $K^{k\theta}(\mathbf{x},t), c_k(\mathbf{x},t)$ will almost at local equilibrium. Meaning the reaction is diffusion controlled. For small $K^{k\theta}(\mathbf{x},t)$ the velocity term will have a significant influence on the concentration, resulting in a reaction controlled system. Having both effects influencing the behaviour is often called the mixed-mode character of the austenite to ferrite transformation kinetics.

2.1.4 Matrix-matrix boundary

The matrix-matrix boundary $\Gamma^{\gamma\alpha}(t)$ is called a grain boundary. This kind of boundary will try to move to a position such that it reduces the total free energy. Next to a local equilibrium, a para-equilibrium could be assumed. This means only one of the concentrations is assumed constant on the interface. Then we need one more condition, this could be a so called mobility condition or a reaction boundary condition like the matrix-precipitate boundary condition.

Local equilibrium

Just like the matrix-precipitate boundary a Dirichlet condition can be chosen.

$$c_\gamma(\mathbf{x},t) = c_{\gamma\alpha}^{\mathrm{sol}}(\mathbf{x},t), \text{ for } \mathbf{x} \in \Gamma^{\gamma\alpha}(t), t > t_0, \quad (2.16)$$
$$c_\alpha(\mathbf{x},t) = c_{\alpha\gamma}^{\mathrm{sol}}(\mathbf{x},t), \text{ for } \mathbf{x} \in \Gamma^{\alpha\gamma}(t), t > t_0, \quad (2.17)$$

where $c_{\gamma\alpha}^{\mathrm{sol}}, c_{\alpha\gamma}^{\mathrm{sol}}$ is the known solubility, or equilibrium concentration, for austenite and ferrite at the interface respectively.

Together with the Stefan conditions (2.4), (2.5) and (2.6) we have enough conditions and can calculate the unknown interface velocity with

$$v_n^{\gamma\alpha}(\mathbf{x},t) = \frac{D_\gamma(\mathbf{x},t)\frac{\partial c_\gamma}{\partial n}(\mathbf{x},t) - D_\alpha(\mathbf{x},t)\frac{\partial c_\alpha}{\partial n}(\mathbf{x},t)}{c^{\text{sol}}_{\alpha\gamma}(\mathbf{x},t) - c^{\text{sol}}_{\gamma\alpha}(\mathbf{x},t)},\ \text{for } \mathbf{x} \in \Gamma^{\gamma\alpha}(t), t > t_0, \quad (2.18)$$

where

$$D_\gamma(\mathbf{x},t)\frac{\partial c_\gamma}{\partial n}(\mathbf{x},t) - D_\alpha(\mathbf{x},t)\frac{\partial c_\alpha}{\partial n}(\mathbf{x},t)$$

is the jump in diffusive flux and

$$c^{\text{sol}}_{\alpha\gamma}(\mathbf{x},t) - c^{\text{sol}}_{\gamma\alpha}(\mathbf{x},t)$$

is the jump in concentration over the interface. $\frac{\partial c_\gamma}{\partial n}(\mathbf{x},t)$ and $\frac{\partial c_\alpha}{\partial n}(\mathbf{x},t)$ can be calculated when the concentrations in $\Omega_\gamma(t)$ and $\Omega_\alpha(t)$ are known.

Just as the matrix-precipitate boundary the Gibbs-Thomson effect can be added to the local equilibrium concentration:

$$c^{\text{sol}}_{\gamma\alpha}(\mathbf{x},t) = c^{\infty}_{\gamma\alpha}(t)\exp\left\{\frac{E_{\gamma\alpha}V^m_\alpha}{R_g T(t)}\kappa^{\gamma\alpha}(\mathbf{x},t)\right\},\ \text{for } \mathbf{x} \in \Gamma^{\gamma\alpha}(t), t > t_0, \quad (2.19)$$

$$c^{\text{sol}}_{\alpha\gamma}(\mathbf{x},t) = c^{\infty}_{\alpha\gamma}(t)\exp\left\{-\frac{E_{\alpha\gamma}V^m_\gamma}{R_g T(t)}\kappa^{\gamma\alpha}(\mathbf{x},t)\right\},\ \text{for } \mathbf{x} \in \Gamma^{\gamma\alpha}(t), t > t_0, \quad (2.20)$$

where $c^{\infty}_{\gamma\alpha}(t), c^{\infty}_{\alpha\gamma}(t)$ is the solubility of $k = \gamma, \alpha$ on the interface in $\Omega_\gamma(t), \Omega_\alpha(t)$ respectively. $E_{\gamma\alpha}, E_{\alpha\gamma}$ is the interface energy, V^m_γ, V^m_α the molar volume of γ, α respectively, R_g the gas constant, $T(t)$ the temperature and $\kappa^{\gamma\alpha}(\mathbf{x},t)$ the sum of the principle curvatures of $\Gamma^{\gamma\alpha}(t)$. Note the minus in the exponent of equation (2.20), this is due the fact that $\kappa^{\gamma\alpha}(\mathbf{x},t) = -\kappa^{\alpha\gamma}(\mathbf{x},t)$.

Grain boundary condition

The Stefan condition (2.6) for the interface $\Gamma^{\gamma\alpha}(t)$ has been derived in the previous section from the mass balance. Instead of two unknowns in the matrix/precipitate boundaries there are now three unknowns, namely $v_n^{\gamma\alpha}(\mathbf{x},t), c_\gamma(\mathbf{x},t)$ and $c_\alpha(\mathbf{x},t)$. As the diffusivity in ferrite of carbon appears to be much greater ($D_\alpha = 8.72 \cdot 10^{-11}$ $\text{m}^2\text{s}^{\text{-}1}$, $D_\gamma = 5.62 \cdot 10^{-13}$ $\text{m}^2\text{s}^{\text{-}1}$ at $T = 995$ K) than that of austenite, we can say that at the austenite ferrite interface the carbon concentration in ferrite $c_\alpha(\mathbf{x},t)$ will be instantly at its equilibrium value $c^{\infty}_{\alpha\gamma}(t)$ or including curvature effect $c^{\text{sol}}_{\alpha\gamma}(\mathbf{x},t)$. So we set

$$c_\alpha(\mathbf{x},t) = c^{\text{sol}}_{\alpha\gamma}(\mathbf{x},t),\ \text{for } \mathbf{x} \in \Gamma^{\gamma\alpha}(t), t > t_0. \quad (2.21)$$

In case of a matrix-matrix boundary, also known as a grain boundary, the interface velocity is commonly [5], [6] expressed as

$$v_n^{\gamma\alpha}(\mathbf{x},t) = M(\mathbf{x},t)\Delta G(\mathbf{x},t), \tag{2.22}$$

where $\Delta G(\mathbf{x},t) \approx \chi\left(c_{\gamma\alpha}^{\mathrm{sol}}(\mathbf{x},t) - c_\gamma(\mathbf{x},t)\right)$ is the driving pressure, $M(\mathbf{x},t)$ is the effective interface mobility containing effects like drag or transformation strain and χ is a proportionality factor. Now we have defined two unknowns on $\Gamma^{\gamma\alpha}(t)$ and are left with a non-linear equation in $c_\gamma(\mathbf{x},t)$, namely

$$\begin{aligned} D_\gamma(\mathbf{x},t)\frac{\partial c_\gamma}{\partial n}(\mathbf{x},t) = -D_\alpha(\mathbf{x},t)\frac{\partial c_\alpha}{\partial n}(\mathbf{x},t) + \\ M(\mathbf{x},t)\chi\left(c_{\gamma\alpha}^{\mathrm{sol}}(\mathbf{x},t) - c_\gamma(\mathbf{x},t)\right)\left(c_{\alpha\gamma}^{\mathrm{sol}}(\mathbf{x},t) - c_\gamma(\mathbf{x},t)\right), \text{ for } \mathbf{x}\in\Gamma^{\gamma\alpha}(t), t > t_0. \end{aligned} \tag{2.23}$$

Reaction boundary condition

Just like the matrix-precipitate boundary a linear reaction flux across the interface can be applied, with flux

$$J_r^{\gamma\alpha}(\mathbf{x},t) = -K^{\gamma\alpha}(\mathbf{x},t)\left(c_{\gamma\alpha}^{\mathrm{sol}}(\mathbf{x},t) - c_\gamma(\mathbf{x},t)\right). \tag{2.24}$$

Together with the Stefan condition there is still one more condition required. Just like the grain boundary condition, a Dirichlet condition on $c_\alpha(\mathbf{x},t)$ can be applied, with

$$c_\alpha(\mathbf{x},t) = c_{\alpha\gamma}^{\mathrm{sol}}(\mathbf{x},t), \text{ for } \mathbf{x}\in\Gamma^{\gamma\alpha}(t), t > t_0. \tag{2.25}$$

As in the case of the grain boundary condition, the driving force is the total jump in concentration on the interface.
Then the Stefan condition becomes:

$$\begin{aligned} D_\gamma(\mathbf{x},t)\frac{\partial c_\gamma}{\partial n}(\mathbf{x},t) - D_\alpha(\mathbf{x},t)\frac{\partial c_\alpha}{\partial n}(\mathbf{x},t) = v_n^{\gamma\alpha}(\mathbf{x},t)\left(c_{\alpha\gamma}^{\mathrm{sol}}(\mathbf{x},t) - c_\gamma(\mathbf{x},t)\right), \\ \text{for } \mathbf{x}\in\Gamma^{\gamma\alpha}(t), t > t_0. \end{aligned} \tag{2.26}$$

The flux terms are:

$$J_r^{\gamma\alpha}(\mathbf{x},t) = -K^{\gamma\alpha}(\mathbf{x},t)\left(c_{\gamma\alpha}^{\mathrm{sol}}(\mathbf{x},t) - c_\gamma(\mathbf{x},t)\right), \tag{2.27}$$

$$J_m^{\gamma\alpha}(\mathbf{x},t) = -c_\gamma(\mathbf{x},t)v_n^{\gamma\alpha}(\mathbf{x},t), \tag{2.28}$$

$$\begin{aligned} J_d^{\gamma\alpha}(\mathbf{x},t) = -D_\gamma(\mathbf{x},t)\frac{\partial c_\gamma}{\partial n}(\mathbf{x},t), \\ \text{for } \mathbf{x}\in\Gamma^{\gamma\alpha}(t), t > t_0. \end{aligned} \tag{2.29}$$

Which give the flux boundary condition:

$$-K^{\gamma\alpha}(\mathbf{x},t)\left(c^{\mathrm{sol}}_{\gamma\alpha}(\mathbf{x},t)-c_\gamma(\mathbf{x},t)\right)=-c_\gamma(\mathbf{x},t)v_n^{\gamma\alpha}(\mathbf{x},t)-D_\gamma(\mathbf{x},t)\frac{\partial c_\gamma}{\partial n}(\mathbf{x},t), \quad \text{for } \mathbf{x}\in\Gamma^{\gamma\alpha}(t), t>t_0. \tag{2.30}$$

Combining the Stefan condition with the flux boundary condition results in:

$$D_\gamma(\mathbf{x},t)\frac{\partial c_\gamma}{\partial n}(\mathbf{x},t)=\frac{D_\alpha(\mathbf{x},t)}{c^{\mathrm{sol}}_{\alpha\gamma}(\mathbf{x},t)}\frac{\partial c_\alpha}{\partial n}(\mathbf{x},t)c_\gamma(\mathbf{x},t)+$$
$$\frac{K^{\gamma\alpha}(\mathbf{x},t)}{c^{\mathrm{sol}}_{\alpha\gamma}(\mathbf{x},t)}\left(c^{\mathrm{sol}}_{\gamma\alpha}(\mathbf{x},t)-c_\gamma(\mathbf{x},t)\right)\left(c^{\mathrm{sol}}_{\alpha\gamma}(\mathbf{x},t)-c_\gamma(\mathbf{x},t)\right), \text{ for } \mathbf{x}\in\Gamma^{\gamma\alpha}(t), t>t_0. \tag{2.31}$$

and

$$v_n^{\gamma\alpha}(\mathbf{x},t)=-\frac{D_\alpha(\mathbf{x},t)}{c^{\mathrm{sol}}_{\alpha\gamma}(\mathbf{x},t)}\frac{\partial c_\alpha}{\partial n}(\mathbf{x},t)+\frac{K^{\gamma\alpha}(\mathbf{x},t)}{c^{\mathrm{sol}}_{\alpha\gamma}(\mathbf{x},t)}\left(c^{\mathrm{sol}}_{\gamma\alpha}(\mathbf{x},t)-c_\gamma(\mathbf{x},t)\right), \quad \text{for } \mathbf{x}\in\Gamma^{\gamma\alpha}(t), t>t_0. \tag{2.32}$$

Comparing this with the grain boundary condition we see that

$$M(\mathbf{x},t)\chi=-\frac{D_\alpha(\mathbf{x},t)}{c^{\mathrm{sol}}_{\alpha\gamma}(\mathbf{x},t)\left(c^{\mathrm{sol}}_{\gamma\alpha}(\mathbf{x},t)-c_\gamma(\mathbf{x},t)\right)}\frac{\partial c_\alpha}{\partial n}(\mathbf{x},t)+\frac{K^{\gamma\alpha}(\mathbf{x},t)}{c^{\mathrm{sol}}_{\alpha\gamma}(\mathbf{x},t)}, \quad \text{for } \mathbf{x}\in\Gamma^{\gamma\alpha}(t), t>t_0. \tag{2.33}$$

This gives us some understanding of the parameters $M(\mathbf{x},t)\chi$ with respect to $K^{\gamma\alpha}(\mathbf{x},t)$. Also note that from this we can see that

$$c_\gamma(\mathbf{x},t)=c^{\mathrm{sol}}_{\gamma\alpha}(\mathbf{x},t)-\frac{1}{K^{\gamma\alpha}(\mathbf{x},t)}\left(v_n^{\gamma\alpha}(\mathbf{x},t)c^{\mathrm{sol}}_{\alpha\gamma}(\mathbf{x},t)-D_\alpha(\mathbf{x},t)\frac{\partial c_\alpha}{\partial n}(\mathbf{x},t)\right), \quad \text{for } \mathbf{x}\in\Gamma^{\gamma\alpha}(t), t>t_0. \tag{2.34}$$

Meaning if $K^{\gamma\alpha}(\mathbf{x},t)$ is large, $c_\gamma(\mathbf{x},t)$ will be close to local equilibrium and the reaction is diffusion controlled. For small $K^{\gamma\alpha}(\mathbf{x},t)$ the velocity term, together with the diffusivity in $\Omega_\alpha(t)$, will have a significant influence on the concentration. Meaning the system is reaction controlled, just like the reaction based boundary condition on $\Gamma^{\gamma\theta}(t)$ and $\Gamma^{\alpha\theta}(t)$.

2.2 Initial solution

In order to have a valid initial solution c_0 for a 1D model, we solve the system, as proposed by den Ouden in [1],

$$\frac{\partial}{\partial x}\left(D_\gamma(x)\frac{\partial}{\partial x}\tilde{c}_\gamma(x)\right) = 0, \text{for } x \in \Omega_\gamma(t_0), \tag{2.35}$$

$$\tilde{c}_\gamma(x) = c_\gamma^0(x), \text{for } x \in \partial\Omega_\gamma(t_0)\backslash\Gamma^{\gamma\alpha}(t_0) \tag{2.36}$$

plus one of the three different interface boundary conditions (Dirichlet, reaction or mobility), for the auxiliary concentration $\tilde{c}_\gamma(x)$. It can be easily seen that for this 1D model the solution for $\tilde{c}_\gamma(x)$ is linear with values c_γ^0 at x_0 and the concentration value satisfying the interface boundary condition at $\Gamma^{\gamma\alpha}(t_0)$. Then we set our initial condition for $c_\gamma(x,t)$ as

$$c_\gamma(x,t_0) = \left(\tilde{c}_\gamma(x) - c_\gamma^0\right) H(x) + c_\gamma^0, \tag{2.37}$$

where the function $H(x)$ is defined as

$$H(x) = \frac{1}{2}\left(1 - \sin\left(\frac{x - \Gamma^{\gamma\alpha}(t_0) - \frac{1}{2}|\Omega_\gamma(t_0)|}{|\Omega_\gamma(t_0)|}\pi\right)\right), \text{for } x \in \Omega_\gamma(t_0). \tag{2.38}$$

This function is zero in x_0 and one in $\Gamma^{\gamma\alpha}(t_0)$ and satisfies a homogeneous Neumann boundary condition in x_0. This means $c_\gamma(x,t_0)$ holds for the no-flux condition on the outer boundary at x_0 and holds for the interface $\Gamma^{\gamma\alpha}(t_0)$ boundary condition. For $T = 995$ K this gives the initial concentration profile as seen in Figure 2.2 and 2.3. $c_\alpha(x,t_0)$ is linear between its local equilibrium concentration at $\Gamma^{\gamma\alpha}(t_0)$ and its reaction equilibrium concentration at $\Gamma^{\alpha\theta}(t_0)$. As the temperature is just below A_1 these are close, but not equal as seen from the phase diagram.

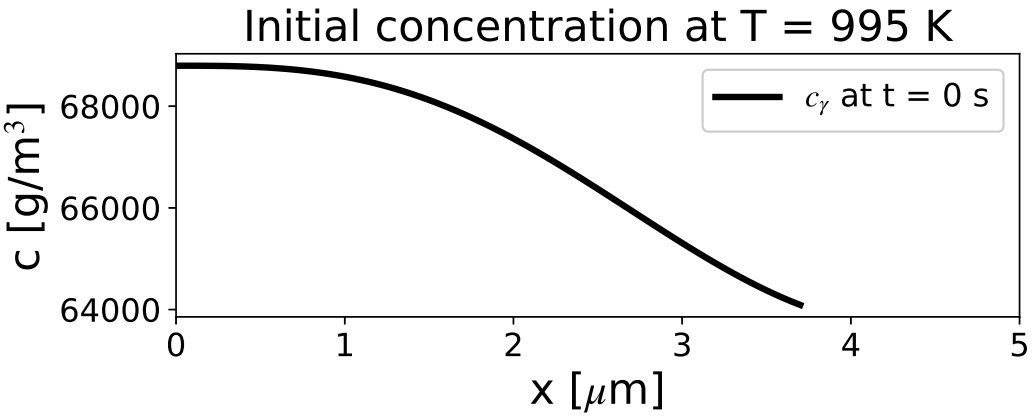

Figure 2.2: Initial concentration of austenite at $t = t_0, T = 995$ K.

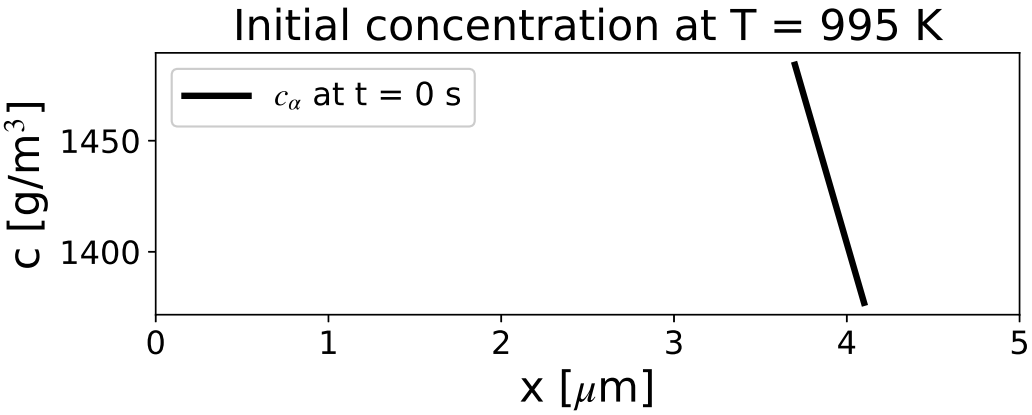

Figure 2.3: Initial concentration of ferrite at $t = t_0, T = 995$ K.

Chapter 3

Boundary moving methods

The biggest problem in approximating Stefan problems is how to keep track of the interface(s), which is part of the models prescription. There are two types of methods being used in today's research. The first type are implicit tracking methods, also called front tracking methods, like the level-set method, the enthalpy method and the phase-field method, which do not use the interface itself but describe it implicitly. The other type of boundary moving methods are explicit tracking methods, called front capturing methods, which keep track of the interface itself.
In this chapter the level-set method is explained and several other methods are presented on how they work and what their advantages and disadvantages are. In this research we will use the implicit level-set method. Why this method is chosen will be made clear from the descriptions below.

3.1 Level-set method

The level-set method captures the movement of an interface $\Gamma^{kl}(t)$ between the domains $\Omega_k(t)$ and $\Omega_l(t)$, by keeping track of a signed-distance function $\phi^{kl}(\mathbf{x}, t)$ defined as:

$$\phi^{kl}(\mathbf{x},t) = \begin{cases} + \min\limits_{\mathbf{y}\in\Gamma^{kl}(t)} ||\mathbf{y}-\mathbf{x}||_2 & \text{, if } \mathbf{x} \in \overline{\Omega_k}(t)\backslash\Gamma^{kl}(t), \\ 0 & \text{, if } \mathbf{x} \in \Gamma^{kl}(t), \\ - \min\limits_{\mathbf{y}\in\Gamma^{kl}(t)} ||\mathbf{y}-\mathbf{x}||_2 & \text{, if } \mathbf{x} \in \overline{\Omega_l}(t)\backslash\Gamma^{kl}(t). \end{cases} \tag{3.1}$$

Note that $\phi^{kl}(\mathbf{x},t)=0$ implicitly implies that $\mathbf{x}$ is located on the interface.
From this definition of $\phi^{kl}(\mathbf{x},t)$ the normal vector of the interface is easily derived,

$$\mathbf{n}^{kl}(\mathbf{x},t)=\frac{\nabla\phi^{kl}(\mathbf{x},t)}{||\nabla\phi^{kl}(\mathbf{x},t)||_2}. \tag{3.2}$$

Then we get the curvature:

$$\kappa^{kl}(\mathbf{x},t)=-\nabla\cdot\mathbf{n}^{kl}(\mathbf{x},t)=-\nabla\cdot\frac{\nabla\phi^{kl}(\mathbf{x},t)}{||\nabla\phi^{kl}(\mathbf{x},t)||_2}. \tag{3.3}$$

The movement of the interface is captured by using the convection equation for evolving the signed-distance function $\phi(\mathbf{x},t)$ over time,

$$\frac{\partial\phi^{kl}}{\partial t}(\mathbf{x},t)+v_n^{\text{ext},kl}(\mathbf{x},t)||\nabla\phi^{kl}(\mathbf{x},t)||_2=0,\ \text{for } \mathbf{x}\in\Omega, t>t_0. \tag{3.4}$$

$v_n^{\text{ext}}(\mathbf{x},t)$ is the normal velocity $v_n^{kl}(\mathbf{x},t)$ of the interface extended over the whole domain. Multiple possible extensions exist for this normal velocity, but to keep this extension simple we solve the Laplace equation

$$\Delta v_n^{\text{ext}}(\mathbf{x},t)=0,\ \text{for } \mathbf{x}\in\Omega, t>t_0 \tag{3.5}$$

with homogeneous Neumann boundary condition on $\partial\Omega$ and Dirichlet condition

$$v_n^{\text{ext},kl}(\mathbf{x},t)=v_n^{kl}(\mathbf{x},t),\ \text{for } \mathbf{x}\in\Gamma^{kl}(t), t>t_0, \tag{3.6}$$

where $v_n^{kl}(\mathbf{x},t)$ is given by the chosen boundary conditions in section 2.1 for $kl\in\{\gamma\theta,\alpha\theta,\gamma\alpha\}$.

3.1.1 Multiple level-set functions

When there are multiple phases in an alloy, more than one level-set function $\phi(\mathbf{x},t)$ is needed. Take for example the sketch of three phases in steel shown in the introduction at $t=t_0$. After some time Δt the phases might look something like below in Figure 3.1.
As seen from this sketch, it is not exactly known how many different level-set functions are required in the implementation of our three phase model, it is one of the questions that we will try to answer this research. [7] is a research done by Xinewie Zhang, Jiun-Shyan Chen and Stanly Osher, which tackles this problem for any material with different phases/grains and implies this is not an arbitrary task.

When two of the same phase types come together and connect, as a phase in between dissolves, the two interfaces connect. No extra conditions have to be set for the connection of two phases, because one level-set function is used per phase or per interface type. Meaning this connection is automatically registered in the function as the values change. See Figure 3.2 as illustration.

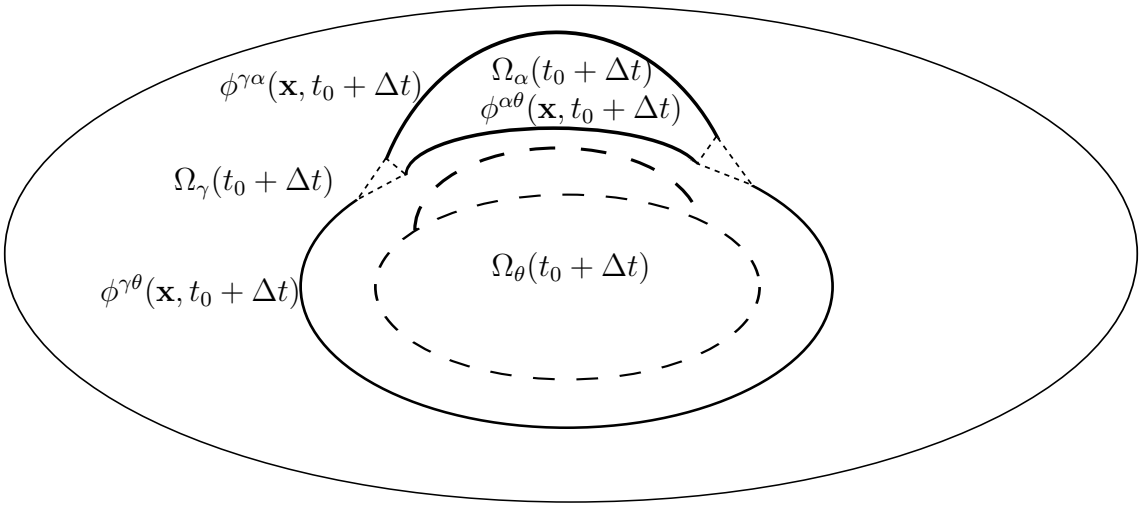

Figure 3.1: A sketch of a just nucleated ferrite phase at $t = t_0$ (dashed lines) on the austenite cementite interface and the same alloy on $t = t_0 + \Delta t$.

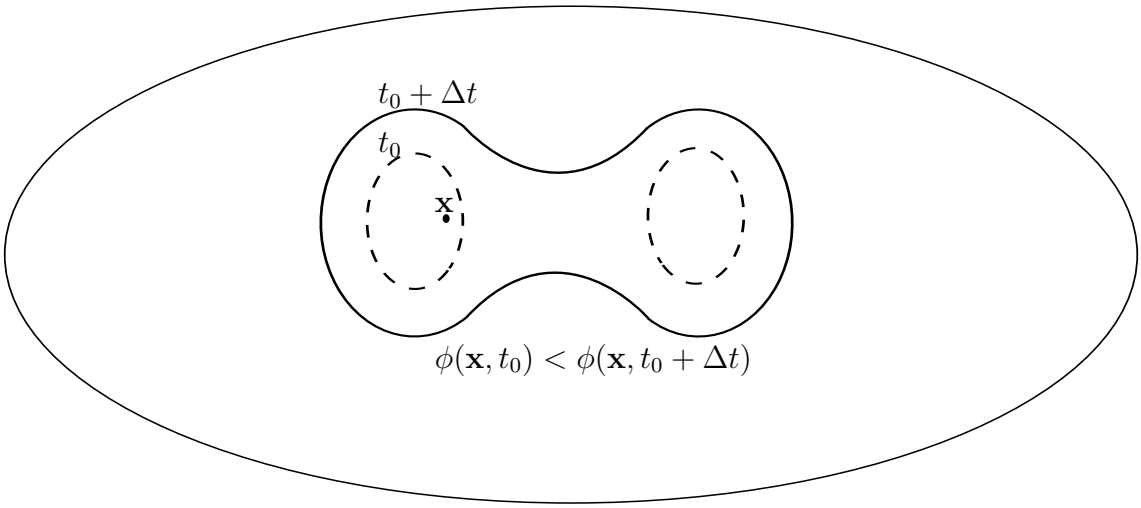

Figure 3.2: When two phases of the same type connect. point $\mathbf{x}$ will get a bigger value for ϕ as the two phases connect.

3.1.2 1D example

Lets consider a simple example in 1D where we have a diffusive domain $\Omega_D(t), t > t_0$, which is on the left of the interface $\Gamma^{Dp}(t), t > t_0$ and a precipitate domain $\Omega_p(t), t > t_0$ on the right of the interface. From the Laplace equation (3.5) for $v_n^{\text{ex},Dp}(x,t)$ we easily see that $v_n^{\text{ex},Dp}(x,t)$ has to be a linear function and even constant, because of the homogeneous Neumann boundary condition. We get:

$$v_n^{\text{ex},Dp}(x,t) = v_n^{Dp}(\Gamma^{Dp}(t),t), \text{ for } x \in \Omega. \tag{3.7}$$

The signed distance function is also easily found as the minimal distance is just the distance between a point x and the interface $\Gamma^{Dp}(t)$:

$$\phi^{Dp}(x,t) = x - \Gamma^{Dp}(t). \tag{3.8}$$

Substituting this in the convection equation (3.4) gives:

$$\frac{\partial \phi^{Dp}}{\partial t}(x,t) = \frac{d\Gamma^{Dp}(t)}{dt}(t) = -v_n^{\text{ex},Dp}(x,t)\left|\frac{\partial \phi^{Dp}(x,t)}{\partial x}\right| = -v_n^{Dp}(\Gamma^{Dp}(t),t). \tag{3.9}$$

Also notice that the curvature $\kappa^{Dp}(x,t)$ is zero as the normal 'vector' $\mathbf{n}^{Dp} = 1$. So it will be impossible to see any curvature effects in a 1D model.

3.2 Other methods

3.2.1 Front-tracking method

A front-tracking method keeps track of the interface explicitly. Next to the computational domain, it has a different set of points that represent the position of the interfaces. These points are updated by moving them with the calculated normal velocity. The location of the interface defines where the material parameters vary on the domain. Some methods also track the line segments and surface segments (in 3D) as objects of the interface changing due to surface tension.

A big problem with explicit front-tracking methods is how to model the fusion of two of the same phases as the interfaces cross each other. As we have three different phases in our model and do not know in advance how they will interact, this event may occur and an implicit method will be more practical. Implicit methods deal with this problem automatically from its definition, as seen for example in the level-set method above.

3.2.2 Front-capturing methods

Enthalpy method

This model is derived from the thermodynamical concepts for heat. A Stefan problem for heat transfer is defined the same as the concentration model described in this paper, but with different parameters and temperature as variable. The enthalpy function $H(t)$ is introduced alongside the heat equations. $H(t)$ is the sum of the specific heat and the latent heat required for a phase change. Substituting the enthalpy function in the heat problem will result in a new problem describing an energy balance combing temperature and enthalpy with a discontinuity at the interface, because of the needed energy to change phase.

It is however impossible to use this method on a model where concentrations are allowed to have a value which lies in between the jump [8]. However, this is one of the driving forces for phase changes in metallurgical problems in the first place. So this method is not viable to use for our model.

Phase-field method

The phase-field method defines an order function $\phi(\mathbf{x}, t)$ per phase type, which is zero outside of its phase domain and one in its domain. At the interface it has a smooth transition between zero and one (See Figure 3.3 [9]).

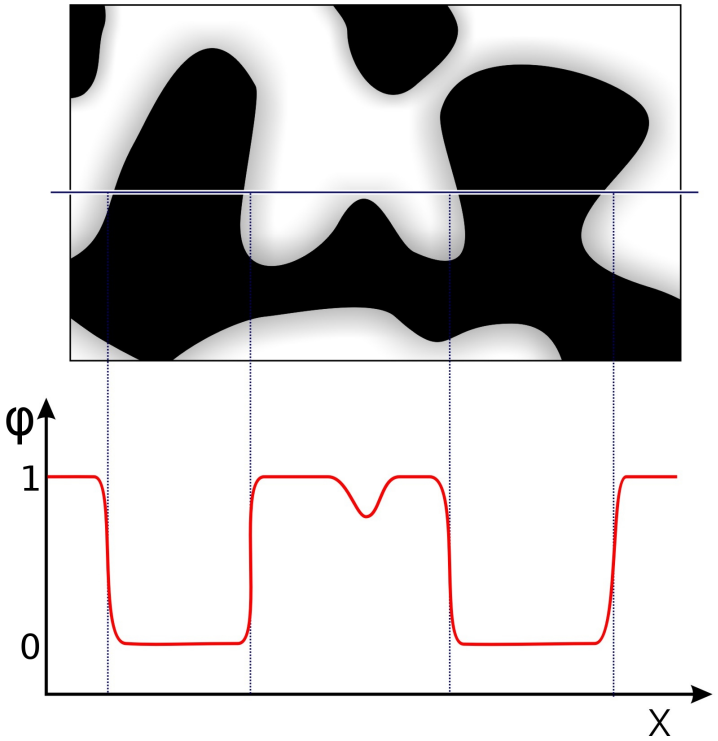

Figure 3.3: Example of a phase-field function $\phi(\mathbf{x}, t)$ for the white phase.

The movement of the phase-field will define the movement of the interfaces. The equation for the change in phase-field is derived from a Helmholtz free energy functional depending on $\phi(\mathbf{x}, t)$ and the physics of the model. It has the same purpose as the convection equation in the level-set method.

The problem with the phase-field method is that the physical parameters needed for the phase-field equation are sometimes difficult to obtain. Furthermore a certain thickness have to be set for the transitions over two different phases, whereas the level-set method has a sharp interface. Also most of the time this thickness is set as an artificial value bigger than physical values for these transition-phases [10].

Chapter 4

Discretisation by Galerkin FEM

Galerkins finite elements method is used to approximate the solution of the Stefan problem. In this chapter we will first derive the weak form for the two diffusive phases Ω_γ and Ω_α with only the Neumann condition on the outer boundary of Ω. Then the different interface boundary conditions will be applied to get the boundary element equations. Lastly two different time discretisation are used and a resulting dimensional problem is treated.

4.1 Weak form

The governing equations of the model are

$$\begin{cases} \frac{\partial c_k}{\partial t}(\mathbf{x},t) &= \nabla \cdot (D_k(\mathbf{x},t)\nabla c_k(\mathbf{x},t)) &, \text{for } \mathbf{x} \in \Omega_k(t), k = \gamma, \alpha, t > t_0, \\ c_\theta(\mathbf{x},t) &= c_\theta &, \text{for } \mathbf{x} \in \Omega_\theta(t), t > t_0, \\ \frac{\partial c}{\partial n}(\mathbf{x},t) &= 0 &, \text{for } \mathbf{x} \in \partial\Omega, t > t_0, \\ c(\mathbf{x},t) &= c_0 &, \text{for } \mathbf{x} \in \Omega, t = t_0, \end{cases} \tag{4.1}$$

where boundary conditions for $\Gamma^{\gamma\alpha}(t), \Gamma^{\gamma\theta}(t), \Gamma^{\alpha\gamma}(t)$ and $\Gamma^{\alpha\theta}(t)$ still have to be set to make the model sufficient and c_0 is the initial concentration profile at $t = t_0$.

For sake of clarity we do not write down the dependence on $\mathbf{x}$ and t in the following equations.
Multiplying the right hand side of the first equation of (4.1) by a test function ψ, which is zero on boundary elements if c_k has a Dirichlet boundary condition, and

integrate over domain Ω_k to get the weak form.

$$\int_{\Omega_k} \psi \frac{\partial c_k}{\partial t} d\Omega = \int_{\Omega_k} \psi \nabla \cdot (D_k \nabla c_k) d\Omega. \tag{4.2}$$

Using Green's first identity we get:

$$\int_{\Omega_k} \psi \frac{\partial c_k}{\partial t} d\Omega = \int_{\partial\Omega_k} \psi D_k \frac{\partial c_k}{\partial n} d\Gamma - \int_{\Omega_k} \nabla\psi \cdot D_k \nabla c_k d\Omega. \tag{4.3}$$

Taking $k = \gamma$ and splitting the boundary integrals to each different interface and using the Neumann condition at the outer boundary gives:

$$\int_{\Omega_\gamma} \psi \frac{\partial c_\gamma}{\partial t} d\Omega = \int_{\Gamma^{\gamma\theta}} \psi D_\gamma \frac{\partial c_\gamma}{\partial n} d\Gamma + \int_{\Gamma^{\gamma\alpha}} \psi D_\gamma \frac{\partial c_\gamma}{\partial n} d\Gamma - \int_{\Omega_\gamma} \nabla\psi \cdot D_\gamma \nabla c_\gamma d\Omega. \tag{4.4}$$

For $k = \alpha$ we get a similar equation:

$$\int_{\Omega_\alpha} \psi \frac{\partial c_\alpha}{\partial t} d\Omega = \int_{\Gamma^{\alpha\theta}} \psi D_\alpha \frac{\partial c_\alpha}{\partial n} d\Gamma + \int_{\Gamma^{\alpha\gamma}} \psi D_\alpha \frac{\partial c_\alpha}{\partial n} d\Gamma - \int_{\Omega_\alpha} \nabla\psi \cdot D_\alpha \nabla c_\alpha d\Omega. \tag{4.5}$$

Equation (4.4) and (4.5) together is the weak form of (4.1).

The different boundary conditions will now be given to make the weak form sufficient.

4.1.1 Matrix/precipitate boundary

Interface reaction

For the matrix/precipitate boundaries, austenite/cementite and ferrite/cementite, an interface reaction boundary condition is taken. This will fix the interface velocity, leaving the austenite and ferrite concentration as variables on the austenite/cementite and ferrite/cementite interfaces respectively.
The $k\theta$-interface term of the weak forms (4.4) and (4.5) become

$$\int_{\Gamma^{k\theta}} \psi D_k \frac{\partial c_k}{\partial n} d\Gamma = \int_{\Gamma^{k\theta}} \psi \frac{K^{k\theta}}{c_\theta} \left(c_\theta - c_k\right) \left(c_{k\theta}^{\mathrm{sol}} - c_k\right) d\Gamma, k = \gamma, \alpha. \tag{4.6}$$

4.1.2 Matrix/matrix boundary

Local equilibrium austenite/ferrite boundary

When local equilibrium for both austenite and ferrite is assumed on the interface $\Gamma^{\gamma\alpha}$, the interface velocity is the unknown quantity. The boundary integral over $\Gamma^{\gamma\alpha}$ in (4.4) becomes

$$\int_{\Gamma^{\gamma\alpha}} \psi D_\gamma \frac{\partial c_\gamma}{\partial n} d\Gamma = 0, \tag{4.7}$$

because the basis function ψ is zero where a Dirichlet boundary condition is assumed. Similarly for (4.5):

$$\int_{\Gamma^{\alpha\gamma}} \psi D_\alpha \frac{\partial c_\alpha}{\partial n} d\Gamma = 0. \tag{4.8}$$

The model with the local equilibrium boundary condition on $\Gamma^{\gamma\alpha}$ and reaction boundary condition on $\Gamma^{\gamma\theta}$ and $\Gamma^{\alpha\theta}$, we will call DDR (DirichletDirichletReaction).

Mobility velocity austenite/ferrite boundary

When a grain mobility condition is assumed on the interface $\Gamma^{\gamma\alpha}$ with para-equilibrium for the ferrite concentration, the boundary integral over $\Gamma^{\gamma\alpha}$ in equation (4.4) becomes

$$\int_{\Gamma^{\gamma\alpha}} \psi D_\gamma \frac{\partial c_\gamma}{\partial n} d\Gamma = \int_{\Gamma^{\gamma\alpha}} \psi \left(D_\alpha \frac{\partial c_\alpha}{\partial n} + M\chi \left(c^{\mathrm{sol}}_{\gamma\alpha} - c_\gamma \right) \left(c^{\mathrm{sol}}_{\alpha\gamma} - c_\gamma \right) \right) d\Gamma \tag{4.9}$$

and $\Gamma^{\alpha\gamma}$ in (4.5):

$$\int_{\Gamma^{\alpha\gamma}} \psi D_\alpha \frac{\partial c_\alpha}{\partial n} d\Gamma = 0. \tag{4.10}$$

The model with the mobility plus para-equilibrium boundary condition on $\Gamma^{\gamma\alpha}$ and reaction boundary condition on $\Gamma^{\gamma\theta}, \Gamma^{\alpha\theta}$ we will call MDR (MobilityDirichletReaction).

Interface reaction austenite/ferrite boundary

When an interface reaction is assumed on the interface $\Gamma^{\gamma\alpha}$, with para-equilibrium for the ferrite concentration, the boundary integral over $\Gamma^{\gamma\alpha}$ in equation (4.4) becomes

$$\int_{\Gamma^{\gamma\alpha}} \psi D_\gamma \frac{\partial c_\gamma}{\partial n} d\Gamma = \int_{\Gamma^{\gamma\alpha}} \psi \left(\frac{D_\alpha}{c^{\mathrm{sol}}_{\alpha\gamma}} \frac{\partial c_\alpha}{\partial n} c_\gamma + \frac{K^{\gamma\alpha}}{c^{\mathrm{sol}}_{\alpha\gamma}} \left(c^{\mathrm{sol}}_{\gamma\alpha} - c_\gamma \right) \left(c^{\mathrm{sol}}_{\alpha\gamma} - c_\gamma \right) \right) d\Gamma \tag{4.11}$$

and $\Gamma^{\alpha\gamma}$ in (4.5):

$$\int_{\Gamma^{\alpha\gamma}} \psi D_\alpha \frac{\partial c_\alpha}{\partial n} d\Gamma = 0. \tag{4.12}$$

The model with the reaction plus para-equilibrium boundary condition on $\Gamma^{\gamma\alpha}$ and reaction boundary condition on $\Gamma^{\gamma\theta}$ and $\Gamma^{\alpha\theta}$, we will call RDR (ReactionDirichletReaction).

4.2 Space discretisation

In this literature study a 1D implementation is used to observe the behaviour of the model and the different boundary conditions. So for this report we will define the mesh generation in a 1D setting. 2D (and 3D) will have a similar approach, but will not be discussed here.

To find the concentration $c_k(\mathbf{x}, t), k = \gamma, \alpha$, we need to find $c_k(\mathbf{x}, t) \in \Sigma$, where

$$\Sigma = \left\{ c_k(\mathbf{x}, t) \text{ sufficiently smooth }, \mathbf{x} \in \Omega_k(t) \,\middle|\, c_k(\mathbf{x}, t) = c^{\text{sol}}(\mathbf{x}, t), \text{for } \mathbf{x} \in \Gamma_k^D(t), t > t_0 \right\},$$

is the solution space and $\Gamma_k^D(t)$ are the interfaces with a Dirichlet boundary condition, such that the weak form (4.4) and (4.5) hold for all

$$\psi(\mathbf{x}) \in \Sigma_0 = \left\{ \psi(\mathbf{x}), \mathbf{x} \in \Omega_k(t), t > t_0 \,\middle|\, \psi(\mathbf{x}) = 0, \text{for } \mathbf{x} \in \Gamma_k^D(t) \right\}.$$

We choose piecewise linear basis functions $\psi_l(\mathbf{x}) \in \Sigma_0, l = 1, \ldots, N_k(t), k = \gamma, \alpha$ defined on a mesh $T_k(t)$. Next we choose an arbitrary, but known function, $c_D(\mathbf{x}, t)$ that satisfies the Dirichlet boundary conditions, like:

$$c_D(\mathbf{x}, t) = c_D^{\text{sol}}(\mathbf{x}, t), \text{for } \mathbf{x} \in \Gamma^D(t), t > t_0. \tag{4.13}$$

We approximate $c_k(\mathbf{x}, t)$ by a finite dimensional subset of Σ as:

$$c_k(\mathbf{x}, t) \approx c_k^{N_k(t)}(\mathbf{x}, t) = \sum_{l=1}^{N_k(t)} \psi_l(\mathbf{x}) c_k^l(t) + c_D(\mathbf{x}, t). \tag{4.14}$$

$T_k(t)$ is a union of $N_k(t) - 1$ disjunct elements $\Omega_k^m(t)$. Subtituting (4.14) in the weak form will result in a general system defined as:

$$M_k(t) \frac{d\mathbf{c}_k(t)}{dt} = S_k\left(t, \mathbf{c}_k(t)\right) \mathbf{c}_k(t) + \mathbf{f}_k\left(t, \mathbf{c}_k(t)\right), k = \gamma, \alpha, t > t_0, \tag{4.15}$$

where element matrix $M_k(t)$ is called the mass matrix, element matrix $S_k\left(t, \mathbf{c}_k(t)\right)$ the stiffness matrix and $\mathbf{f}_k\left(t, \mathbf{c}_k(t)\right)$ the right hand side vector.

As ferrite nucleates on the interface of austenite and cementite, we assume ferrite to be in the middle of the three phaces of a one dimensional line. Define a background mesh T on Ω and assume we know the position of the interfaces $\Gamma^{\gamma\alpha}(t)$ and $\Gamma^{\alpha\theta}(t)$. The interfaces define which part of the background mesh belongs to the diffusive domains $\Omega_\gamma(t)$ and $\Omega_\alpha(t)$ by looking at the sign of the values from the level-set functions for the diffusive phases. However, as we have a one dimensional mesh it is easy to see which elements and points belong to which phase without looking at the level-set functions, thus we neglect this for now, although it will be needed in higher dimensional implementations.
The interfaces themselves are added as grid points dividing the element the interface is in, in two new elements. Now we have created the diffusive meshes $T_\gamma(t)$ and $T_\alpha(t)$. However, in order to avoid very small elements, meaning the interface is close to an original grid point $x_i \in T_k(t)$, we shift that grid point to the interface. We define

$$\frac{|x_i - \Gamma^{kl}(t)|}{|\Omega_{\Gamma^{kl}}(t)|} \leq \delta, kl \in \{\gamma\alpha, \alpha\theta\}, \tag{4.16}$$

where $|\Omega_{\Gamma^{kl}(t)}|$ is the length of the element $\Gamma^{kl}(t)$ is in. If this inequality holds, the grid point x_i gets shifted to $\Gamma^{kl}(t)$, if not $\Gamma^{kl}(t)$ is added as a new point to the respective diffusive mesh. In this research we have chosen $\delta = 0.3$. See Figure 4.1 as illustration.

4.2.1 Satisfying dimensions

As an interface moves, a grid point of the original mesh can be shifted to the interface on some time t^n satisfying the inequality (4.16). Whereas one time step Δt later, at t^{n+1}, it will be out of range to satisfy the inequality (4.16). This means that in the domain $\Omega_k(t^{n+1}) = \Omega_k^{n+1}$ this grid point is in, the domain suddenly gets an extra point and thus element. If $N_k(t^n) = N_k^n$ is the amount of points in Ω_k^n, $N_k^{n+1} = N_k^n + 1$ in this case.
In the next section about time discretisation we will see that a matrix-vector multiplication is needed between a matrix at the new time t^{n+1} and a vector at the old time t^n. The event just described tells us the dimensions of these two objects will not satisfy. To make this matrix-vector multiplication valid again, we need to somehow extend the vector to the mesh at this new time. Three different techniques

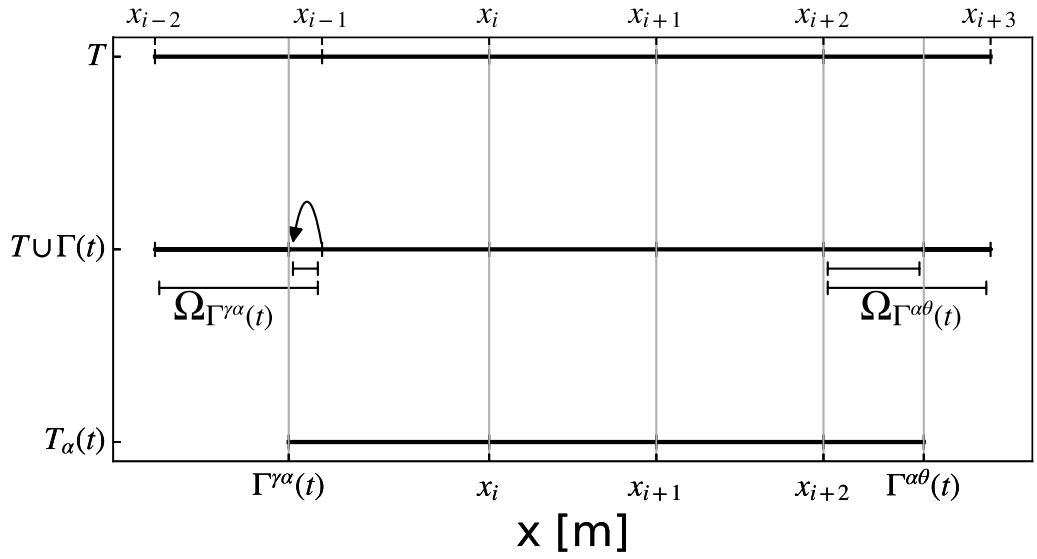

Figure 4.1: 1D example with the part of the background mesh T that covers $\Omega_\alpha(t)$ and an illustration of a shift from x_{i-1} to $\Gamma^{\gamma\alpha}(t)$ and a point x_{i+2} not shifted to the interface $\Gamma^{\alpha\theta}(t)$.

will be given below. These techniques will be based around moving one or more grid points of T_k^n to the locations of T_k^{n+1}.

Shift point

The easiest way to extend the solution $\mathbf{c}_k^n$, as done by den Ouden in [1], is to set:

$$\forall \mathbf{x}_i \in T_k^{n+1}, i = 1, \ldots, N_k^{n+1}, k = \gamma, \alpha \text{ find } \min_{\mathbf{y}_i \in T_k^n} ||\mathbf{x}_i - \mathbf{y}_i||_2, \quad i = 1, \ldots, N_k^n, k = \gamma, \alpha. \tag{4.17}$$

An index-to-index function $I : i \to j$ will indicate which point $\mathbf{y}_j$ is closest to point $\mathbf{x}_i$. The extended solution vector $\mathbf{c}_{k,\text{ex}}^n$ is then given by

$$\left(\mathbf{c}_{k,\text{ex}}^n\right)_i = \left(\mathbf{c}_k^n\right)_{I(i)}. \tag{4.18}$$

As most points in T_k^n of a diffusive phase Ω_k^n will not be shifted from the background mesh T until an interface gets close to it, we have $\mathbf{x}_i = \mathbf{y}_i$ for most i.

From the index-to-index function we can also easily define a mesh velocity $\mathbf{v}_k^{\text{mesh}}$ as

$$\left(\mathbf{v}_k^{\text{mesh}}\left(t^{n+1}\right)\right)_i = \frac{\mathbf{y}_{I(i)} - \mathbf{x}_i}{\Delta t}, i = 1, \ldots, N_k^{n+1}, k = \gamma, \alpha. \tag{4.19}$$

See Figure 4.2 for an example of the domain Ω_k^n and Ω_k^{n+1}. Here a new point emerged in the mesh T_α^{n+1}, because of the movement of $\Gamma^{\gamma\alpha}(t)$. The new point is closest to $\Gamma^{\gamma\alpha}(t^n)$ on the old mesh T_α^n.
It turns out that most of the time, if not always, the new point is closest to the interface on the old mesh, because the time step Δt is chosen depending on the interface velocity such that the interface will never jump 'too' far. This means the concentration for the extended solution on x_{new} is the concentration on $\Gamma^{\gamma\alpha}(t^n)$. This point has a Dirichlet boundary condition, meaning the concentration will become fixed by the Dirichlet prescription. This is not something we want, so we look at two other techniques below.

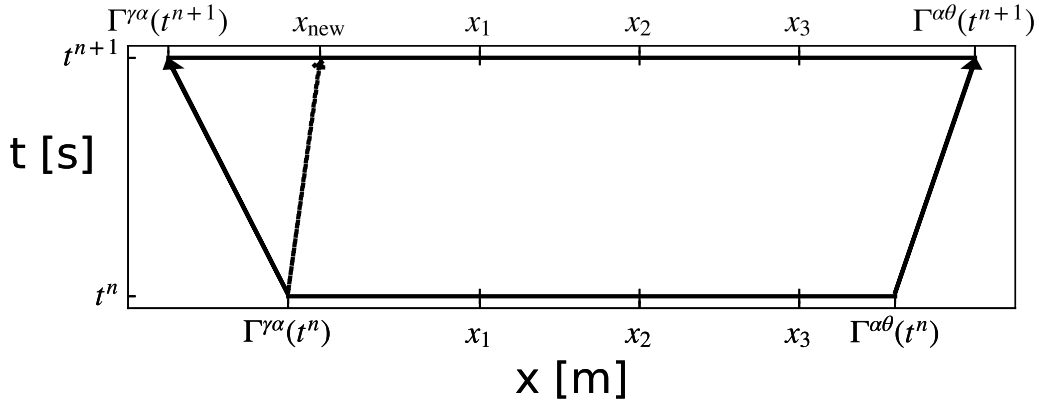

Figure 4.2: Meshes T_α^n and T_α^{n+1} where a new point x_{new} emerged, because of the movement of the interface $\Gamma^{\gamma\alpha}$. This new point is defined to originate from the closest point of the mesh on t^n, namely $\Gamma^{\gamma\alpha}(t^n)$. Also note that there is no new point from the movement of $\Gamma^{\alpha\theta}(t^n)$.

Interpolate point

With the shift technique, the concentration assigned to a 'new' point $x_{\text{new}} \in T_k^{n+1}$ considered on the mesh T_k^n is not the same as the concentration value when assuming a piecewise linear function, which we have for $c_k^{N_k^n}(\mathbf{x}, t^n)$. Also, frequently, the point

closest to x_{new} on the old mesh T_k^n is an interface point, where the concentration can be fixed because of a Dirichlet condition.
Instead of assuming the points origin is a mesh point on the previous mesh, the point can be assumed to come from somewhere within the element containing the interface and given the concentration by using the piecewise linear concentration function. This way, technically, no mass is added to the system. The point of origin x_{old} for the new point x_{new} is taken as

$$x_{\text{old}} = (x_{\text{new}} - x_i) \frac{\left|\Omega_{k,i}^n\right|}{\left|\Omega_{k,i}^{n+1}\right|} + x_i, \tag{4.20}$$

where x_i is the other mesh point of the boundary element $\Omega_{k,i}^n$ and $\Omega_{k,i}^n$. See Figure 4.3 for an example with $i = 1$ and $k = \alpha$.

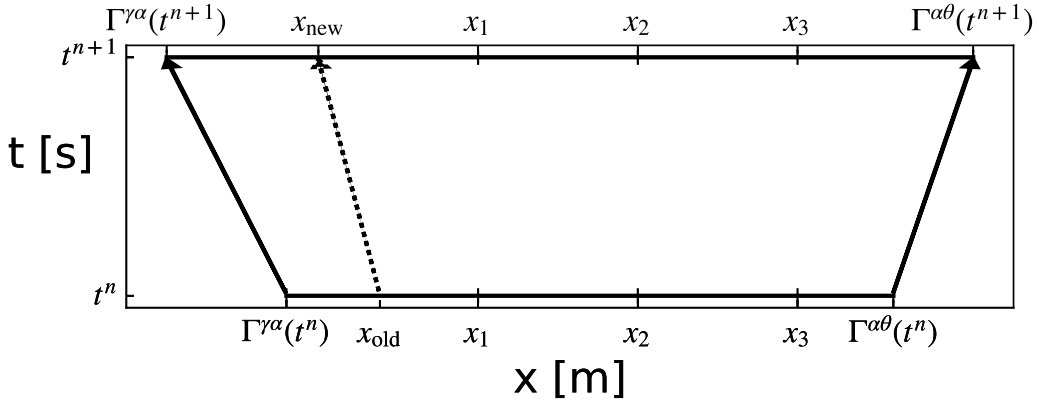

Figure 4.3: Meshes T_α^n and T_α^{n+1} where a new point x_{new} emerged, because of the movement of the interface $\Gamma^{\gamma\alpha}(t^n)$. The point is defined to originate from within the interval $(\Gamma^{\gamma\alpha}(t^n), x_1)$ scaled to the interval $(\Gamma^{\gamma\alpha}(t^{n+1}), x_1)$.

See Figure 4.4 below for the concentration function $c_{\alpha,\text{ex}}^n(x)$ compared to $c_\alpha^n(x)$ in a 1D example when the shift point technique (dotted line) and the interpolate point technique (line with square points) is used.

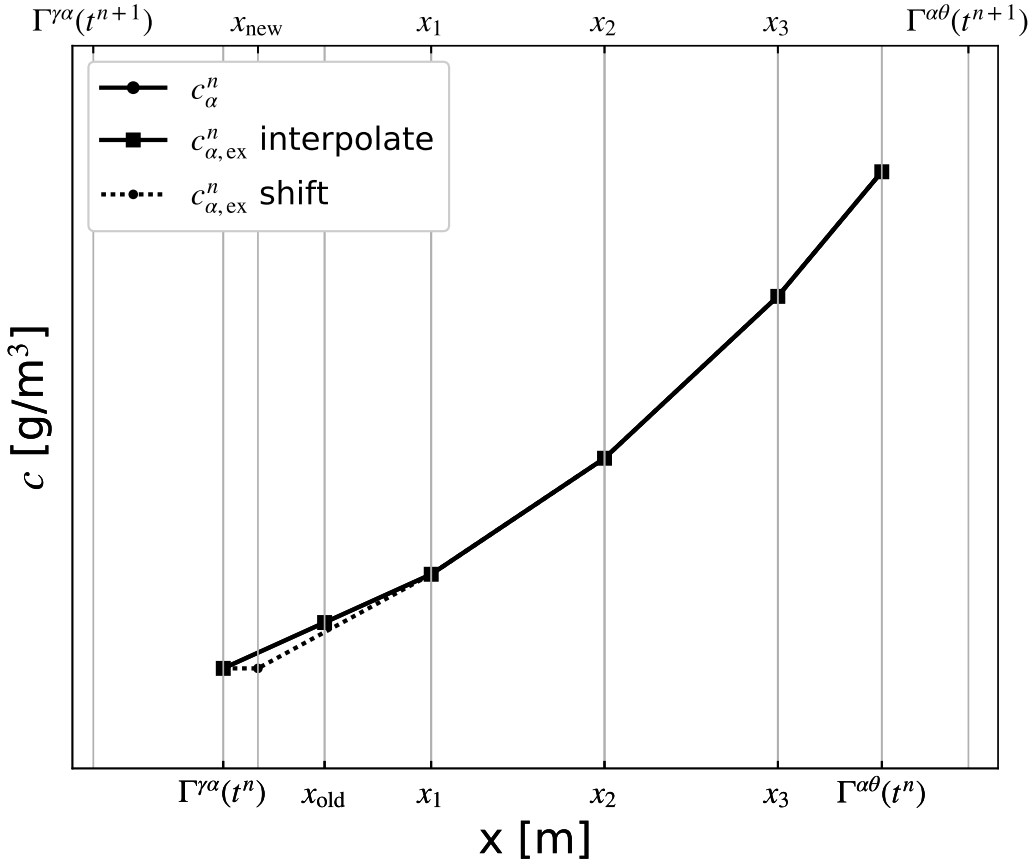

Figure 4.4: Concentration of $c_{\alpha,\text{ex}}^n$ with the shift-point technique compared to $c_{\alpha,\text{ex}}^n$ with interpolation technique.

L2-projection

A more refined method is the so-called L2-projection. In this case all points of the new mesh are supposed to have moved over time. Just like the interpolation technique a point is moved by looking at the ratios as in (4.20). Not the ratio of one element though, but of the whole domain $\frac{|\Omega_k^n|}{|\Omega_k^{n+1}|}$. See Figure 4.5 as example.

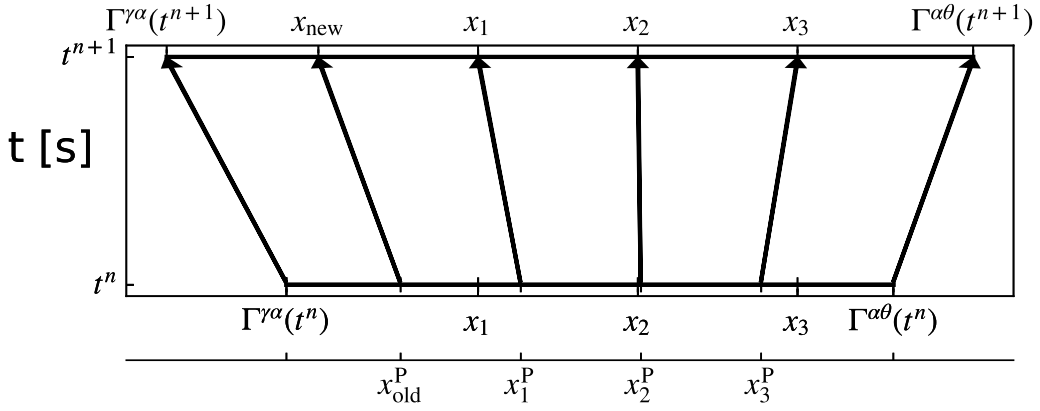

Figure 4.5: x^P represent the points projected with factor $\frac{\left|\Omega_k^n\right|}{\left|\Omega_k^{n+1}\right|}$.

Then the concentrations are calculated by requiring mass conservation. Meaning

$$\int_{\Omega_k^n} c_{k,\text{ex}}^n(\mathbf{x}) d\mathbf{x} = \int_{\Omega_k^n} c_k^n(\mathbf{x}) d\mathbf{x}, \tag{4.21}$$

but also

$$\int_{\Omega_k^n} \lambda(\mathbf{x}) c_{k,\text{ex}}^n(\mathbf{x}) d\mathbf{x} = \int_{\Omega_k^n} \lambda(\mathbf{x}) c_k^n(\mathbf{x}) d\mathbf{x} \tag{4.22}$$

for any function $\lambda(\mathbf{x})$. So also for $\lambda(\mathbf{x}) = \psi_{i,\text{ex}}^n(\mathbf{x}), i = 1, \ldots, N_k^n$, the basis function on the extended mesh of T_k^n.
With

$$c_k^n(\mathbf{x}) = \sum_{l=1}^{N_k^n} \psi_l^n(\mathbf{x}) \left(\mathbf{c}_k^n\right)_l,$$

and

$$c_{k,\text{ex}}^n(\mathbf{x}) = \sum_{l=1}^{N_k^{n+1}} \psi_{l,\text{ex}}^n(\mathbf{x}) \left(\mathbf{c}_{k,\text{ex}}^n\right)_l,$$

(4.22) transforms to:

$$\sum_{l=1}^{N_k^{n+1}} \int_{\Omega_k^n} \psi_{i,\text{ex}}^n(\mathbf{x}) \psi_{l,\text{ex}}^n(\mathbf{x}) \left(\mathbf{c}_{k,\text{ex}}^n\right)_l d\mathbf{x} = \sum_{l=1}^{N_k^n} \int_{\Omega_k^n} \psi_{i,\text{ex}}^n(\mathbf{x}) \psi_l^n(\mathbf{x}) \left(\mathbf{c}_k^n\right)_l d\mathbf{x}, \tag{4.23}$$

or

$$M_{\text{ex}}^n \mathbf{c}_{\text{ex}}^n = \mathbf{m}\left(\mathbf{c}^n\right), \tag{4.24}$$

where M_{ex}^n is the extended mass matrix on time t^n and $\mathbf{m}\left(\mathbf{c}^n\right)_i^{\Omega_k^n} = \int_{\Omega_k^n} \psi_{i,\text{ex}}^n(\mathbf{x}) c^n(\mathbf{x}) d\mathbf{x}$, which is approximated, for example, by Gaussian Legendre quadrature [11]. One could also use the fact that $\mathbf{c}^n$ is a piecewise linear function to derive a more simple approximation method than the Gaussian Legendre quadrature.
The extended concentration with L2-projection compared to the interpolation technique is shown in Figure 4.6 below. Both methods produce an extended solution similar to the original solution and both preserve mass.

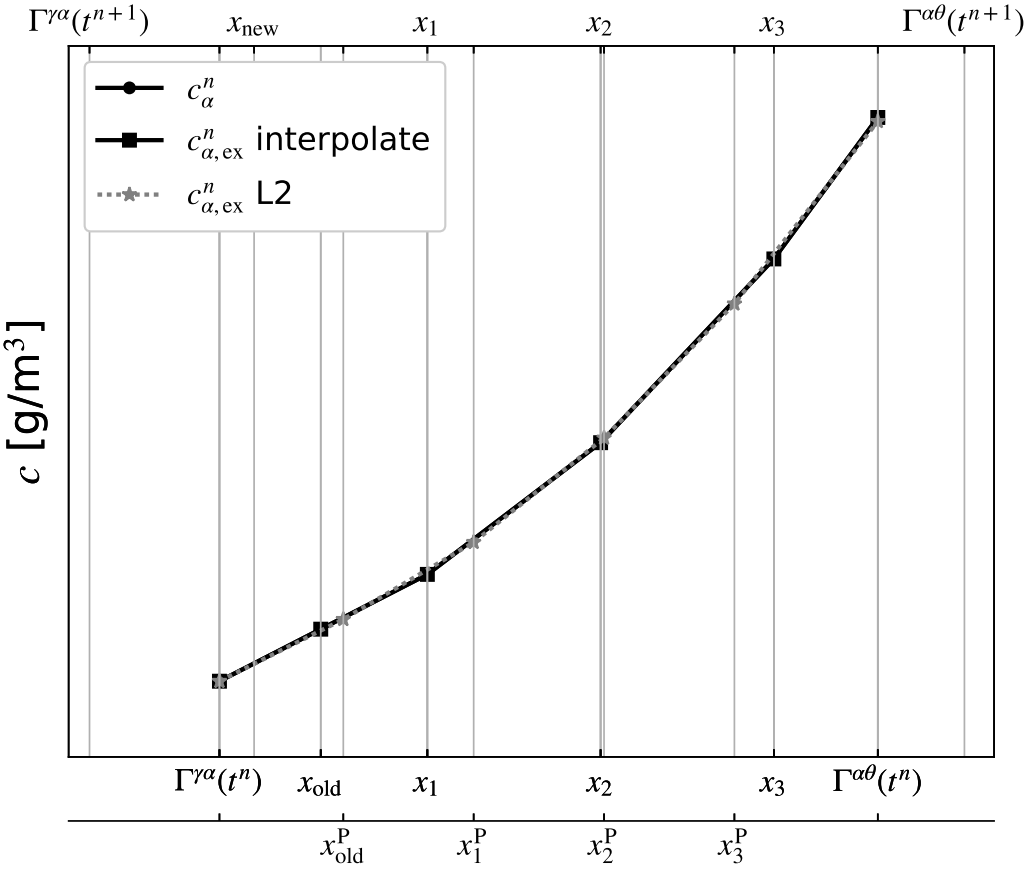

Figure 4.6: Concentration of $c_{\alpha,\text{ex}}^n$ with L2-projection compared to $c_{\alpha,\text{ex}}^n$ with interpolation technique. x^P represent the points projected with factor $\frac{\left|\Omega_k^n\right|}{\left|\Omega_k^{n+1}\right|}$.

4.3 Time discretisation

In this section we consider two different approximation methods for the time integration, implicit Euler and Crank-Nicolson. Of course more methods can be considered, but a negative property of higher order methods pushes us to favour the simpler implicit Euler method.

4.3.1 First order implicit Euler

First order implicit Euler on equation (4.15) gives the system for $\mathbf{c}_k(t)$ as

$$\left(M_k\left(t^{n+1}\right) - \Delta t S_k\left(t^{n+1}, \mathbf{c}_k^{n+1}\right)\right)\mathbf{c}_k^{n+1} = M_k\left(t^{n+1}\right)\mathbf{c}_k^n + \Delta t \mathbf{f}_k\left(t^{n+1}, \mathbf{c}_k^{n+1}\right). \quad (4.25)$$

Δt is the chosen time step from t^n to t^{n+1}. This approximation results in a first order accurate time integration. The implicit Euler method, or also called the backward Euler method, is unconditionally stable, making it a perfect candidate. Furthermore the implicit Euler method preserves positivity if (4.25) is solved exactly. This means no oscillations can occur in the solutions.

Satisfying dimensions

If we have N_k^n grid points on time $t = t^n$ in the diffusive phase mesh T_k^n for $k = \gamma, \alpha$ it is certainly possible that N_k^{n+1} can be a different value, as described in the previous section about space discretisation. This results in a mismatch in the matrix-vector multiplication between $M_k\left(t^{n+1}\right)$ and $\mathbf{c}_k^n$. To fix this mismatch we will extend the solution $\mathbf{c}_k^n$ from the mesh T_k^n to T_k^{n+1}. Three different techniques for this extending process have been given in subsection 4.2.1. These techniques extend the solution vector by assuming the new arisen point, or even all points in the new mesh, has/have moved from somewhere in the old mesh to the new mesh. By this movement of points, convection is introduced to the system. To take in account this convection we must replace the partial derivative in our system of equations (4.1) with a material derivative. The material derivative is defined as

$$\frac{Dc_k}{Dt}(\mathbf{x}, t) = \frac{\partial c_k}{\partial t}(\mathbf{x}, t) + \frac{d\mathbf{x}}{dt}(t) \cdot \nabla c_k(\mathbf{x}, t), \quad (4.26)$$

which will turn equation (4.1) into

$$\begin{cases} \frac{Dc_k}{Dt}(\mathbf{x},t) &= \nabla\cdot(D_k(\mathbf{x},t)\nabla c_k(\mathbf{x},t)) + \frac{d\mathbf{x}}{dt}(t)\cdot\nabla c_k(\mathbf{x},t) &, \text{for } \mathbf{x}\in\Omega_k(t), k=\gamma,\alpha,\\ c_\theta(\mathbf{x},t) &= c_\theta &, \text{for } \mathbf{x}\in\Omega_\theta(t),\\ \frac{\partial c_k}{\partial n}(\mathbf{x},t) &= 0 &, \text{for } \mathbf{x}\in\partial\Omega_k(t), t>t_0,\\ c(\mathbf{x},t) &= c_0 &, \text{for } \mathbf{x}\in\Omega, t=t_0. \end{cases} \tag{4.27}$$

The velocity of a point $\mathbf{x}$ at time t^{n+1} will be approximated by the mesh velocity $\mathbf{v}_k^{\text{mesh}}(t^{n+1})$, created by moving the grid points as described above. This new term will be included in the stiffness matrix $S_k(t,\mathbf{c}_k(t))$. The FEM system we will need to solve is:

$$\left(M_k\left(t^{n+1}\right) - \Delta t S_k\left(t^{n+1},\mathbf{c}_k^{n+1}\right)\right)\mathbf{c}_k^{n+1} = M_k\left(t^{n+1}\right)\mathbf{c}_{k,\text{ex}}^{n} + \Delta t\mathbf{f}_k\left(t^{n+1},\mathbf{c}_k^{n+1}\right). \tag{4.28}$$

4.3.2 Second order Crank-Nicolson and θ-method

To obtain a second order accurate time integration one could, for example, consider Crank-Nicolson. This method combines the first order Implicit-Euler with the first order Explicit-Euler and is unconditionally stable [12].
Say you have the system of equations

$$\frac{\partial c}{\partial t}(\mathbf{x},t) = F\left(c,\mathbf{x},t,\nabla c,\nabla^2 c\right), \tag{4.29}$$

then Crank-Nicolson approximates $\frac{\partial c}{\partial t}(\mathbf{x},t)$ as

$$\frac{c^{n+1}-c^n}{\Delta t} = \frac{1}{2}\left[F^{n+1}\left(c,\mathbf{x},t,\nabla c,\nabla^2 c\right) + F^n\left(c,\mathbf{x},t,\nabla c,\nabla^2 c\right)\right]. \tag{4.30}$$

In our case we get the system

$$\begin{aligned}\left(M_k\left(t^{n+1}\right) - \frac{\Delta t}{2}S_k\left(t^{n+1},\mathbf{c}_k^{n+1}\right)\right)\mathbf{c}_k^{n+1} &= M_k\left(t^{n+1}\right)\mathbf{c}_k^n + \frac{\Delta t}{2}\mathbf{f}_k\left(t^{n+1},\mathbf{c}_k^{n+1}\right)\\ &+\frac{\Delta t}{2}M_k\left(t^{n+1}\right)M_k^{-1}\left(t^n\right)\left[S_k\left(t^n,\mathbf{c}_k^n\right)\mathbf{c}_k^n + \mathbf{f}_k\left(t^n,\mathbf{c}_k^n\right)\right], k=\gamma,\alpha. \end{aligned}\tag{4.31}$$

Note that there are now two more multiplication mismatches, namely in

$$M_k\left(t^{n+1}\right)\left[M_k^{-1}\left(t^n\right)S_k\left(t^n,\mathbf{c}_k^n\right)\mathbf{c}_k^n\right],$$

and

$$M_k\left(t^{n+1}\right)\left[M_k^{-1}\left(t^n\right)\mathbf{f}_k\left(t^n,\mathbf{c}_k^n\right)\right].$$

This implies extended matrices $M_k\left(t^n\right), S_k\left(t^n, \mathbf{c}_k^n\right)$ and extended vectors $\mathbf{f}_k\left(t^n, \mathbf{c}_k^n\right), \mathbf{c}_k^n$ on the new mesh are needed when Crank-Nicolson time integration approximation is used. Next to that the inverse of $M_{k,\mathrm{ex}}\left(t^n\right)$ has to be calculated, three more matrices and one more vector must be constructed per time step and one matrix-matrix product plus two more matrix-vector products have to be calculated. The pro of this method is its second order accuracy, which means bigger time steps Δt can be taken to obtain the same accuracy as a first order approximation. Meaning the extra work needed per time step is cut by doing this work less often. In practice however it appears that oscillations can occur in the solution when $D\Delta t$ is large compared to the (average) grid size Δx squared [13]. This effect we observe in our results in section 6.3. This is why we will use the less accurate, but unconditionally stable and oscillation resistant, Implicit-Euler time integration. Another option would be to use the θ-method. This method takes a combination of Euler forward -and backward with weight θ and $\theta - 1$ respectively for $\theta \in [0, 1]$. The time discretisation for (4.15) with the θ-method reads:

$$\begin{aligned}\left(M_k\left(t^{n+1}\right) - \theta\Delta t S_k\left(t^{n+1}, \mathbf{c}_k^{n+1}\right)\right)\mathbf{c}_k^{n+1} &= M_k\left(t^{n+1}\right)\mathbf{c}_k^n + \theta\Delta t\mathbf{f}_k\left(t^{n+1}, \mathbf{c}_k^{n+1}\right) \\ &+(1-\theta)\Delta t M_k\left(t^{n+1}\right) M_k^{-1}\left(t^n\right)\left[S_k\left(t^n, \mathbf{c}_k^n\right)\mathbf{c}_k^n + \mathbf{f}_k\left(t^n, \mathbf{c}_k^n\right)\right], k = \gamma, \alpha. \quad (4.32)\end{aligned}$$

Note that for $\theta = \frac{1}{2}$ we get the second order Crank-Nicolson method. For any other $\theta \in [0, 1]$ this method will have order one of convergence, but might be close to order two for θ values close to $\theta = \frac{1}{2}$.

Satisfying dimensions

As stated above more extensions are needed for the Crank-Nicolson method and also for the more general θ-method. The FEM system we will need to solve is:

$$\begin{aligned}\left(M_k\left(t^{n+1}\right) - \theta\Delta t S_k\left(t^{n+1}, \mathbf{c}_k^{n+1}\right)\right)\mathbf{c}_k^{n+1} &= M_k\left(t^{n+1}\right)\mathbf{c}_{k,\mathrm{ex}}^n + \theta\Delta t\mathbf{f}_k\left(t^{n+1}, \mathbf{c}_k^{n+1}\right) \\ &+(1-\theta)\Delta t M_k\left(t^{n+1}\right) M_{k,\mathrm{ex}}^{-1}\left(t^n\right)\left[S_{k,\mathrm{ex}}\left(t^n, \mathbf{c}_{k,\mathrm{ex}}^n\right)\mathbf{c}_{k,\mathrm{ex}}^n + \mathbf{f}_{k,\mathrm{ex}}\left(t^n, \mathbf{c}_{k,\mathrm{ex}}^n\right)\right], \\ &k = \gamma, \alpha (4.33)\end{aligned}$$

Chapter 5

Physical parameters

In our model we have introduced several physical parameters which influence the model's behaviour. In order to see if our model resembles the physical model, these parameters are required. Some values can be easily found in literature, but some have to be derived under certain assumptions. In this chapter we will give all parameters together with introducing their temperature/time dependency.

Because temperature drops below the eutectoid temperature A_1, austenite will start dissolving and fully disappear in time with ferrite replacing it, ferrite will nucleate and grow. The biggest driving force behind the dissolve/growth process is that the carbon concentrations tries to spread out evenly, being in equilibrium, while the temperature drops. The concentration it will attain in equilibrium depends on temperature, making the system temperature dependent. As we decrease the temperature over time, temperature is dependent on time. The parameters $K^{k\theta}(\mathbf{x}, t), K^{\gamma\alpha}(\mathbf{x}, t)$ and $M(\mathbf{x}, t)$ are the coefficients that influence the speed of this driving force and are assumed to be only temperature dependent, thus implicitly time dependent.
The other carbon transporting process in our model is diffusion. Diffusion wants to spread out the carbon concentration evenly over the domain. The rate of this diffusion is dependent of the diffusion coefficient $D_k(\mathbf{x}, t)$. The higher temperature, the faster atoms can move, thus the diffusion coefficient tends to be bigger at higher temperatures. So $D_k(\mathbf{x}, t)$ is implicitly time-dependent. We will assume it has the same value for all $\mathbf{x} \in \Omega_k(t)$, meaning it is location independent $D_k(\mathbf{x}, t) = D_k(t)$.

5.1 Local equilibrium concentration

At a temperature just above the eutectoid temperature $A_1 = 1000K$, with a carbon composition between 0.76 and 6.67 wt%, there will be two phases in steel, austenite (γ) and cementite (θ). The carbon equilibrium composition $\text{wt}_{kl}(T(t))\%$ -or concentration $c^{\infty}_{kl}(T(t)), kl \in \{\gamma\alpha, \gamma\theta, \alpha\gamma, \alpha\theta\}$ values can be found in the phase diagram of steel by looking at the given temperature and the equilibrium lines of the different phases (see Figure 5.1).

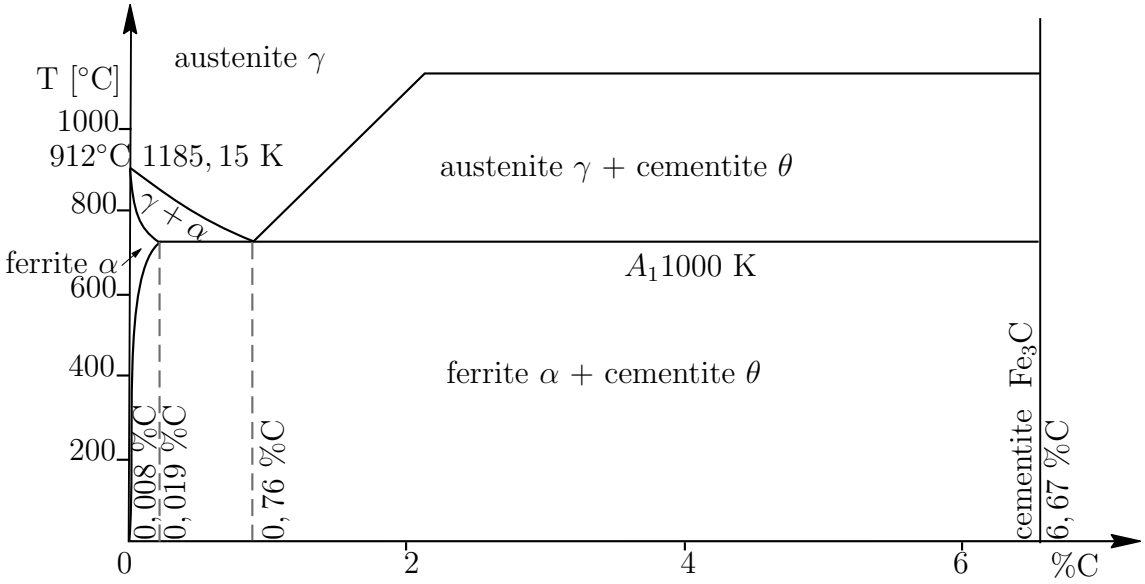

Figure 5.1: Phase diagram of steel.

The moment the temperature drops below A_1 it is expected that ferrite will be created, but not immediately as it will need some amount of free energy available on an interface of austenite and cementite to create the BCC structure. This energy threshold is known as the latent heat.
As seen in the phase diagram, there are no equilibrium composition/concentration values for austenite below A_1. This is to be expected, as at this temperature all austenite will be dissolved when equilibrium is attained. We do however need equilibrium values for boundaries between austenite and ferrite and between austenite and cementite at temperatures below A_1. We can obtain these values by extrapolating the equilibrium lines found in the phase diagram above A_1. From data obtained by ThermoCALC we got the following fits:

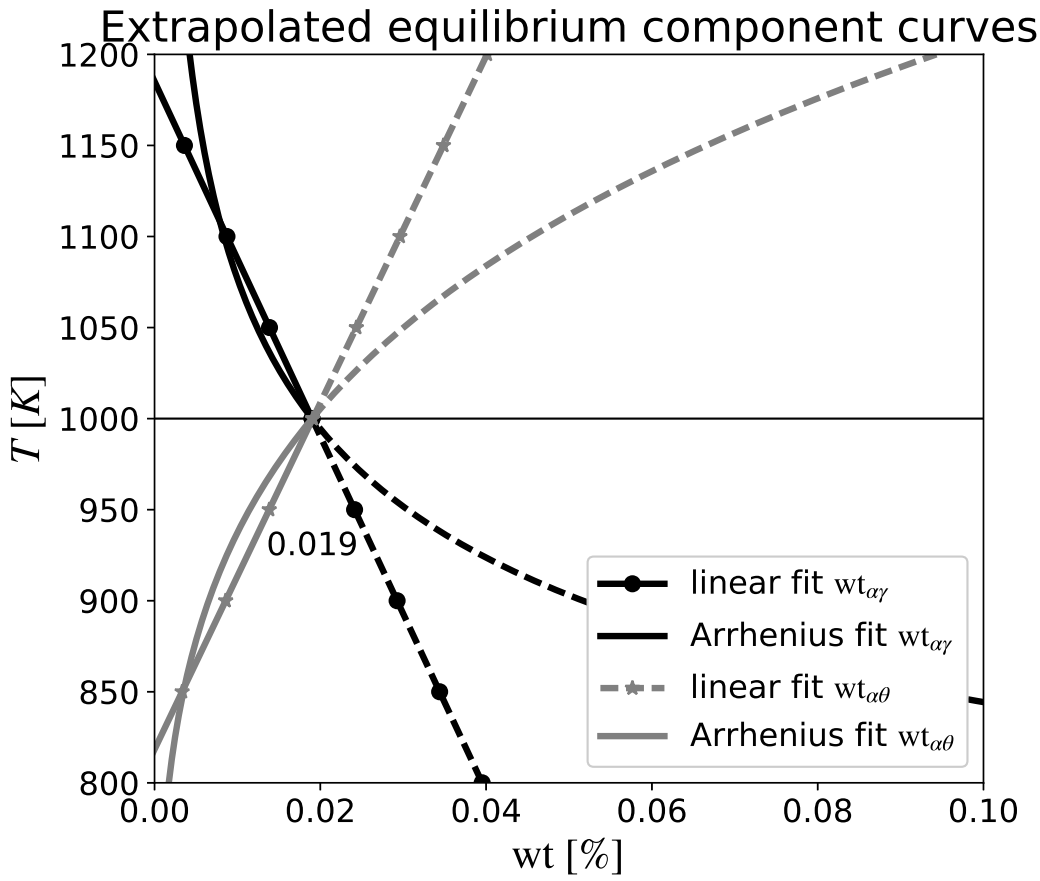

Figure 5.2: Component values for $\mathrm{wt}_{\alpha\gamma}(T(t))\%$ and $\mathrm{wt}_{\alpha\theta}(T(t))\%$ fitted linearly and with an Arrhenius relation. Here the markers do not represent the data-points.

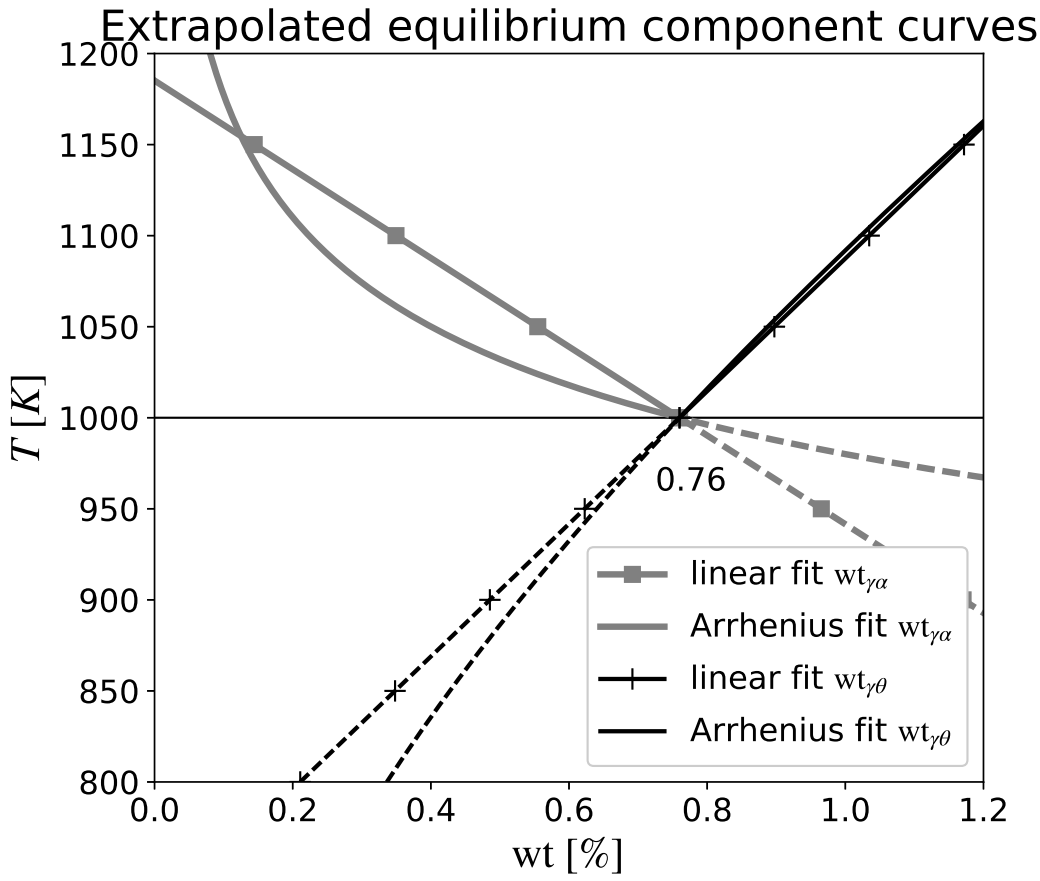

Figure 5.3: Component values for $\mathrm{wt}_{\gamma\alpha}(T(t))\%$ and $\mathrm{wt}_{\gamma\theta}(T(t))\%$ fitted linearly and with an Arrhenius relation. Here the markers do not represent the data-points.

These exponentially curved lines follow the Arrhenius equation [14], which is known as

$$c_{kl}^{\infty}(T(t)) = A \exp\left\{\frac{-E_{\Gamma^{kl}}}{R_g T(t)}\right\}, kl \in \{\gamma\alpha, \gamma\theta, \alpha\gamma, \alpha\theta\}, \tag{5.1}$$

where A is a pre-exponential factor, depending on the frequency of collision of the reaction, $E_{\Gamma^{kl}}$ the interface energy, R_g the gas constant and $T(t)$ the temperature. To see which extrapolation of the data points fits best, we look at the error between the data points and the fit $|\mathrm{wt}_{kl}^{\infty} - \mathrm{fit}\,(\mathrm{wt}_{kl}^{\infty})|_2$:

Error	Linear fit	Arrhenius fit
$\left\|\mathrm{wt}_{\gamma\alpha}^{\infty} - \mathrm{fit}\left(\mathrm{wt}_{\gamma\alpha}^{\infty}\right)\right\|_2$	$8.5 \cdot 10^{-2}$	$7.1 \cdot 10^{-2}$
$\left\|\mathrm{wt}_{\gamma\theta}^{\infty} - \mathrm{fit}\left(\mathrm{wt}_{\gamma\theta}^{\infty}\right)\right\|_2$	$2.4 \cdot 10^{-2}$	$4.6 \cdot 10^{-3}$
$\left\|\mathrm{wt}_{\alpha\gamma}^{\infty} - \mathrm{fit}\left(\mathrm{wt}_{\alpha\gamma}^{\infty}\right)\right\|_2$	$3.61 \cdot 10^{-17}$	$2.6 \cdot 10^{-3}$
$\|\mathrm{wt}_{\alpha\theta}^{\infty} - \mathrm{fit}\,(\mathrm{wt}_{\alpha\theta}^{\infty})\|_2$	$2.7 \cdot 10^{-2}$	$7.6 \cdot 10^{-4}$

Table 5.1: Error between data-points and linear/Arrhenius fit.

From these errors we decide to use the Arrhenius extrapolation data for $\gamma\theta$ and $\alpha\theta$. $\gamma\alpha$ Arrhenius fit does have a lower error, but not significantly. The high values for higher temperatures does not seem to fit the equilibrium line of phase diagram, whereas the linear fit does this better. Fot this reason we choose a linear extrapolation for this equilibrium line. For these values the model works and gives reasonable results. Later on more data could be used to get better Arrhenius fits, but it is not in the scope of this research.

5.1.1 From composition -to concentration values

Most databases and researches on steel phase transformation work with carbon component percentages. In this research we want to stick close the International System of Units (SI) to have a better apprehension of the models solution. Component percentages values can be converted to concentration values by the following formula:

$$c_k = N_k^{\mathrm{atoms}} \frac{M_{\mathrm{Fe}}}{a_k^3} \frac{\mathrm{wt}_k}{1 - \mathrm{wt}_k}, k = \gamma, \alpha, \tag{5.2}$$

where N_k^{atoms} is effective the number of iron atoms present in a unit cell of steel in phase k, M_{Fe} is the molar mass of iron, a_k is the lattice length of a unit cell

in phase k. As austenite is FCC (face-centered cubic), $N_\gamma^{\text{atoms}} = 4$ and ferrite is BCC (body-centered cubic) gives $N_\alpha^{\text{atoms}} = 2$. Cementite does not have a cubic cell, thus it is difficult to find a formula for cementite as presented here. We choose $c_\theta = 7730.14\frac{\text{wt}_\theta}{1-\text{wt}_\theta}\text{kg m}^{-3}$ and $\text{wt}_\theta = 6\frac{2}{3}\%$, where 7730.14 kg m^{-3} is the density of all cementite including iron.

5.2 Other parameters

5.2.1 Diffusion coefficient

The diffusion coefficient follows the same Arrhenius relation as the equilibrium concentrations:

$$D_k(T(t)) = D_{0,k} \exp\left\{\frac{-Q_k}{R_g T(t)}\right\}, \tag{5.3}$$

where $D_{0,k}$ is the diffusion coefficient at infinite temperature, Q_k the activation energy for diffusion, R_g the gas constant and $T(t)$ the temperature at time t. For $k = \gamma$ we have $D_{0,\gamma} = 1.5 \cdot 10^{-5}$ m^{2}s^{-1} and $Q_\gamma = 142.1 M_{\text{Fe}}$ kJg^{-1}, for $k = \alpha$ we have $D_{0,\alpha} = 2.2 \cdot 10^{-4}$ m^{2}s^{-1} and $Q_\alpha = \frac{122.5}{M_{\text{Fe}}}$ kJg^{-1} [5]. The gas constant is an universal constant given by $R_g = \frac{8.31}{M_{\text{Fe}}}$ JK^{-1}g^{-1} [16].

5.2.2 Reaction velocity

In the research of den Ouden [1], $K^{\gamma\theta}(\mathbf{x}, t)$ is chosen proportional to the Debye frequency of carbon multiplied by the distance an atom jumps. The Debye frequency is used in theoretical estimates of rates of diffusion and is considered to be proportional to the diffusivity coefficient $D_k(T(t))$ of carbon divided by the square of the lattice parameter of the phase (γ in his case). The jump distance is proportional with the lattice parameter a_k. As the only variable parameter given for this reaction velocity is $D_k(T(t))$, K^{kl} is also only dependent on $t/T(t)$. All this gives

$$K^{k\theta}(T(t)) = k_{0,k\theta} a_k \frac{D_k(T(t))}{a_k^2} = k_{0,k\theta} \frac{D_k(T(t))}{a_k}, k = \gamma, \alpha, \tag{5.4}$$

with $k_{0,k\theta}$ a proportionality constant, which increases the influence of the reaction term in the mixed-mode transformation character of the model. Similarly, the reaction velocity defined on the interface $\Gamma^{\gamma\alpha}(t)$ is the velocity of the carbon atoms in γ, so we get

$$K^{\gamma\alpha}(T(t)) = k_{0,\gamma\alpha} \frac{D_\gamma(T(t))}{a_\gamma}. \tag{5.5}$$

5.2.3 Interface mobility and proportionality factor

The interface mobility coefficient $M(\mathbf{x}, t)$ is said to also follow an Arrhenius relation

$$M(\mathbf{x}, t) = M(T(t)) = M_0 \exp\left\{\frac{-Q}{R_g T(t)}\right\}, \tag{5.6}$$

with activation energy $Q = \frac{140}{M_{\text{Fe}}}$ kJg^{-1} [5]. The proportionally factor χ is just like $k_{0,kl}$ in the reaction boundary condition and used as a value to fit the model to experimental data and increases the interface controlled physics of the model if increased.

5.3 Temperature cooling rates

At low carbon iron steels (below 0.76 carbon wt %), at the start of the process the interface is found to be controlling the transformation of austenite to ferrite. Over time the diffusion gradually takes over. The rate of transition of interface to diffusion control depends on the cooling rate $\frac{dT}{dt}(t)$ [5]. We will consider different cooling rates to see if the same holds for higher carbon steels (0.6 to 2.0 %). 0.05 Ks^{-1} is considered a low cooling rate, 0.4 Ks^{-1} medium and 10 Ks^{-1} high. We will assume that the temperature decreases linearly from T_0 to T_{end} with a cooling rate somewhere between the low and high value and stays constant at T_{end} for some time to let the model attain equilibrium.

Chapter 6

Results

In this research the following parameters will be used when not specifically specified:

Parameter	Value	Unit	Reference
x_0	0	μm	Chosen
x_N	5	μm	Chosen
N	401	-	Chosen
t_0	0	s	Chosen
t_{end}	$(T_0 - T_{\text{end}})/\frac{dT}{dt}(t)$	s	Chosen
$\Gamma^{\gamma\alpha}(t_0)$	3.7	μm	Chosen
$\Gamma^{\alpha\theta}(t_0)$	4.1	μm	Chosen
$\frac{dT}{dt}(t)$	0.4	Ks^{-1}	[5]
$k_{0,\gamma\alpha}, k_{0,\alpha\theta}$	1	-	Chosen
T_0	995	K	Chosen
T_{end}	800	K	Chosen
$D_{0,\alpha}$	$2.2 \cdot 10^{-4}$	m^{2}s^{-1}	[5]
$D_{0,\gamma}$	$1.5 \cdot 10^{-5}$	m^{2}s^{-1}	[5]
M_{Fe}	55.845	gmol^{-1}	[15]
Q_α	$122.5/M_{\text{Fe}}$	kJg^{-1}	[5]
Q_γ	$142.1/M_{\text{Fe}}$	kJg^{-1}	[5]
R_g	$8.31/M_{\text{Fe}}$	JK^{-1}g^{-1}	[16]
a_γ	$0.36 \cdot 10^{-3}$	μm	[17]
a_α	$0.29 \cdot 10^{-3}$	μm	[17]
wt$_\theta$	6.67	wt % C	Figure 5.1
$c_{\theta,\text{Fe3C}}$	7730.14	kgm^{-3}	Chosen
c_γ^0	$1.1 \cdot c_{\gamma\alpha}^\infty(T_0)$	gm^{-3}	Chosen

Table 6.1: Physical parameters and initial setting for the dissolution of austenite.

t_{end} is the moment the simulation is (assumed) to be in equilibrium state. It is taking as 1.5 times the moment that the temperature reaches $T = T_{\text{end}}$. c_γ^0 is the carbon concentration of austenite on the outer boundary at $t = t_0$.

6.1 Comparing boundary conditions

In the setup of the model we introduced three different boundary conditions for the austenite/ferrite interface. In order to pick one, we will look at simulations done with a one dimensional implementation. First we will compare the Dirichlet with the reaction boundary condition for the austenite concentration on the interface and then compare the reaction with the mobility condition.

6.1.1 DDR compared with RDR

If we increase the proportionality factor $k_{0,\gamma\alpha}$ in $K^{\gamma\alpha}(T(t))$ we should expect the RDR (ReactionDirichletReaction) model to resemble the DDR (DirichletDirichletReaction) model. For smaller values the reaction term will influence the behaviour. In Figure 6.1 the concentration profiles for $c_\gamma(\mathbf{x}, t)$ are shown for several times and with different $k_{0,\gamma\alpha}$. The ★-symbols represent the equilibrium concentrations $c_{\gamma\alpha}^{\text{sol}}(T(t))$. Clearly the high proportionality factor $k_{0,\gamma\alpha} = 1 \cdot 10^2$ and even normal value $k_{0,\gamma\alpha} = 1$ show that the austenite concentration on the austenite/ferrite interface is almost in equilibrium, meaning the boundary condition resembles a Dirichlet boundary condition. Only for a lower proportionality factor $k_{0,\gamma\alpha} = 1 \cdot 10^{-2}$ we see that the austenite concentration clearly has a different value from its equilibrium concentration.
The difference in concentration is easily notable in the concentration figures. There is however no observable difference in the overall behaviour of the model, as we can see in the interface velocities and interface positions in Figure 6.2.

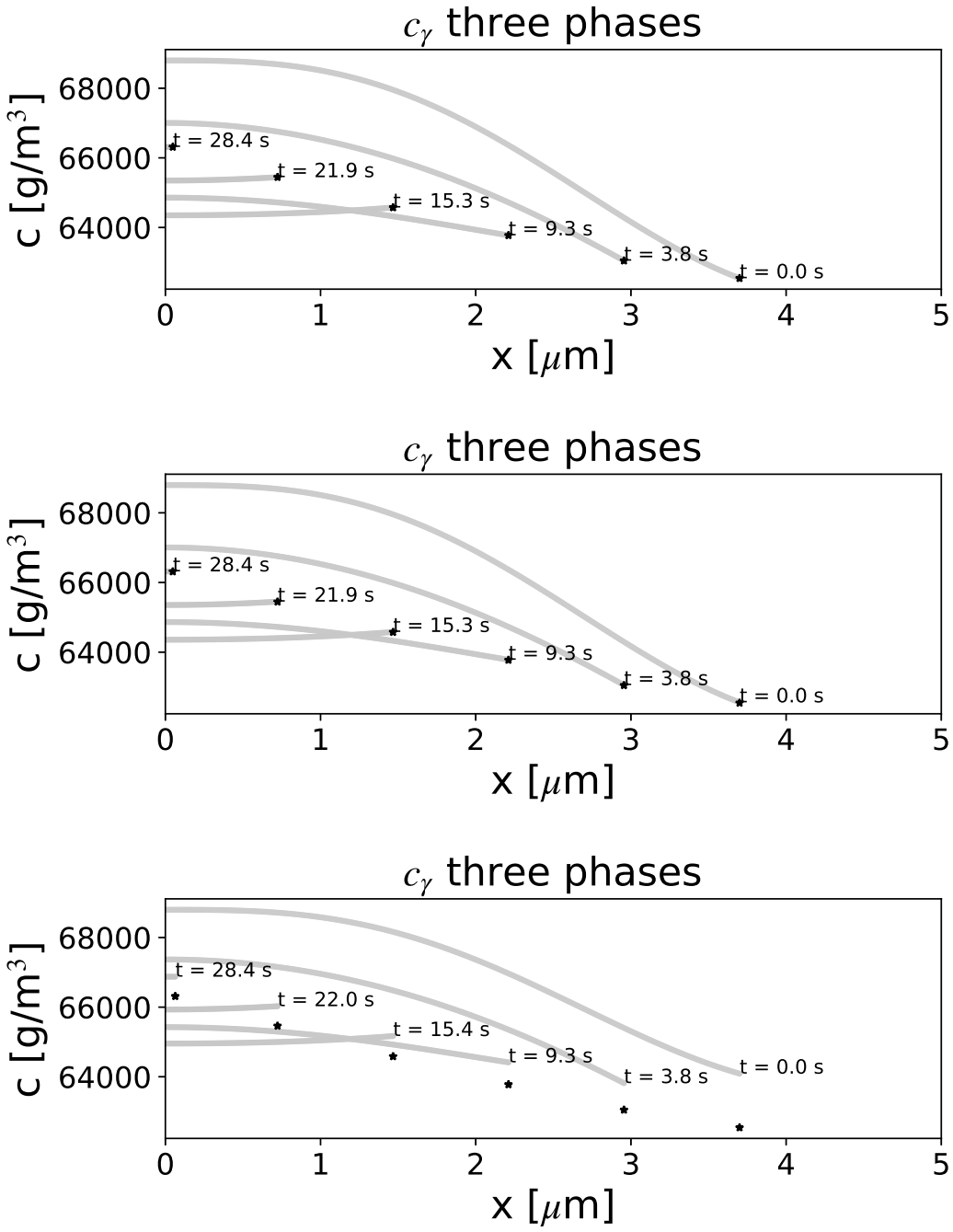

Figure 6.1: Concentration profiles for $k_{0,\gamma\alpha} = 1 \cdot 10^2$ (upper), $k_{0,\gamma\alpha} = 1$ (center) and $k_{0,\gamma\alpha} = 1 \cdot 10^{-2}$ (bottom). The ★-markers represent the equilibrium concentration $c^{\text{sol}}_{\gamma\alpha}(T(t))$.

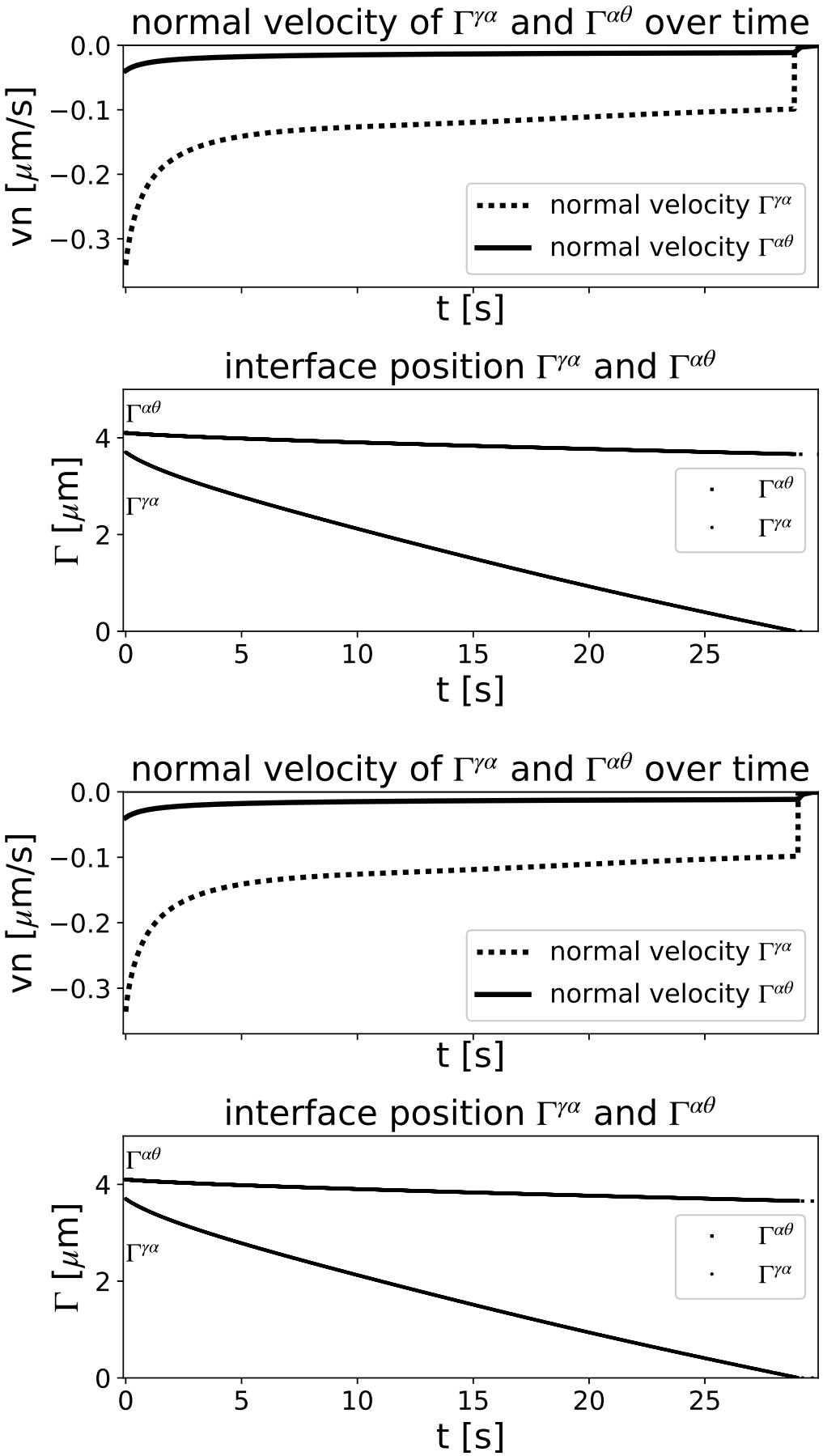

Figure 6.2: Interface velocity and position profiles for $k_{0,\gamma\alpha} = 1 \cdot 10^{2}$ (upper) and $k_{0,\gamma\alpha} = 1 \cdot 10^{-2}$ (bottom).

6.1.2 Mobility parameter (MDR) compared to reaction parameter (RDR)

When introducing the mobility -and reaction boundary condition on $\Gamma^{\gamma\alpha}(t)$, we noticed that there is a relation between $K^{\gamma\alpha}(T(t))$ and $M(T(t))\chi$. This relation is

$$M(T(t))\chi = -\frac{D_\alpha(T(t))}{c^{\text{sol}}_{\alpha\gamma}(T(t))\left(c^{\text{sol}}_{\gamma\alpha}(T(t)) - c_\gamma(\mathbf{x},t)\right)}\frac{\partial c_\alpha}{\partial n}(\mathbf{x},t) + \frac{K^{\gamma\alpha}(T(t))}{c^{\text{sol}}_{\alpha\gamma}(T(t))}, \quad \text{for } \mathbf{x} \in \Gamma^{\gamma\alpha}(t) t > t_0. \tag{6.1}$$

We also know that $M(T(t))$ follows the Arrhenius relation

$$M(T(t)) = M_0 \exp\left\{\frac{-Q}{R_g T(t)}\right\}, \tag{6.2}$$

with $Q = \frac{140}{M_{\text{Fe}}}$ kJg^{-1}, the activation energy and M_0 the mobility coefficient at infinite temperature. Both relations are shown below for a cooling rate of 0.4 Ks^{-1}.

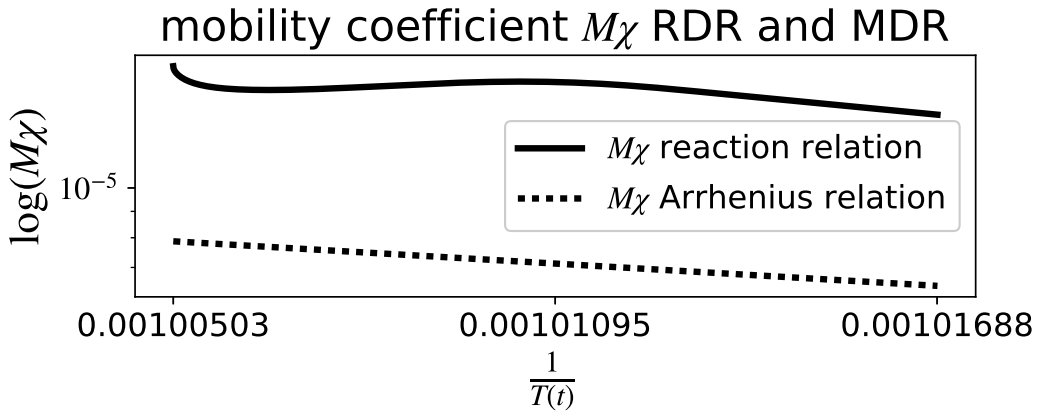

Figure 6.3: $M(T(t))\chi$ plotted as the Arrhenius relation against the relation with $K^{\gamma\alpha}(T(t))$.

The mobility parameter calculated from (6.1) has an activation energy $Q = \frac{232}{M_{\text{Fe}}}$, which is close to the activation energy of the Arrhenius relation in the work of Mecozzi [5]. $M_0\chi = 392.7$ ms^{-1}g^{-1} for the reaction relation and $M_0 = 2.4 \cdot 10^{-6}$ gmJ^{-1}s^{-1}, $\chi = 7.4 \cdot 10^7$ Jm^{3}wt^{-1} [5], gives $M_0\chi = 177.6$ ms^{-1}g^{-1} for the Arrhenius relation. This is an average factor of 2.2 difference with the Arrhenius relation. Naturally, it is expected that these values are not exactly equal. In the work of

Mecozzi a two -and three dimensional model of low carbon steel is modelled, where ferrite grows in austenite and no cementite is present. This could influence the mobility parameter values. Also because the model is higher dimensional, there is a bigger contact surface area between the two phases. The parameters $M_0\chi$ have to compensate this by having a bigger value, which we see from the calculated values for $M_0\chi$ in equation (6.1).

6.2 Convergence and dimensional extension

In order to see if the solving method is correct we need to show it converges. Besides showing the algorithm converges, we first show the accuracy results of the different dimensional extension methods. To show the quality of the algorithm, we look at the error in mass as we know the real mass at t_0 and we know that mass should be conserved.
First we will look at the results for the different extension techniques.

mesh size h μm	Shift point	Interpolate point	L2-projection
0.25	$3.950 \cdot 10^{-2}$	$3.950 \cdot 10^{-2}$	$3.941 \cdot 10^{-2}$
0.125	$3.231 \cdot 10^{-2}$	$3.226 \cdot 10^{-2}$	$3.226 \cdot 10^{-2}$
0.0625	$1.518 \cdot 10^{-2}$	$1.518 \cdot 10^{-2}$	$1.515 \cdot 10^{-2}$
0.03125	$1.203 \cdot 10^{-2}$	$1.202 \cdot 10^{-2}$	$1.201 \cdot 10^{-2}$
0.015625	$7.623 \cdot 10^{-3}$	$7.623 \cdot 10^{-3}$	$7.615 \cdot 10^{-3}$
0.0078125	$3.687 \cdot 10^{-3}$	$3.692 \cdot 10^{-3}$	$3.678 \cdot 10^{-3}$
0.00390625	$2.302 \cdot 10^{-3}$	$2.302 \cdot 10^{-3}$	$2.302 \cdot 10^{-3}$
0.001953125	$1.310 \cdot 10^{-3}$	$1.318 \cdot 10^{-3}$	$1.317 \cdot 10^{-3}$
Calculated order	0.72	0.72	0.72

Table 6.2: Absolute error in mass loss per extension method for several mesh sizes with total mass 0.7439 g at t_{end}.

Not much difference in the methods, as the amount of times an extension is needed is not too frequent and only with a maximal of two points, whereas the total amount of grid points ranges from 21 to 2156. With higher dimensions, more interface points will be present and the extension methods might have more effect. For the rest of the results we will use the interpolate point technique, as this method is relatively less time consuming and almost as accurate as you would expect from the L2-projection. The shift-point technique, should in theory, be a worse option over the other two

as mass is created/deleted. However we do not see much difference in the results, also because mass is created at the austenite/ferrite interface and deleted on the ferrite/cementite interface with the shift-point technique. The extra runtime in the L2-projection technique comes from the extra loop in calculating the $\mathbf{m}(\mathbf{c})$ vector (equation (4.24)) and solving a system of equations to obtain the extended solution.

To compute the order of convergence, we calculate the relative error for several mesh sizes h. We also show the relative error for different start and ending times t_0, t_{end}.

mesh size h (μm)	start: 3, end: 2 phases	start: 3, end: 3 phases	start: 2, end: 2 phases [1]
0.25	$5.309 \cdot 10^{-2}$	$2.310 \cdot 10^{-3}$	$5.832 \cdot 10^{-2}$
0.125	$4.343 \cdot 10^{-2}$	$4.923 \cdot 10^{-4}$	$4.524 \cdot 10^{-2}$
0.0625	$2.040 \cdot 10^{-2}$	$1.732 \cdot 10^{-4}$	$2.091 \cdot 10^{-2}$
0.03125	$1.617 \cdot 10^{-2}$	$5.909 \cdot 10^{-5}$	$1.644 \cdot 10^{-2}$
0.015625	$1.025 \cdot 10^{-2}$	$1.457 \cdot 10^{-5}$	$9.319 \cdot 10^{-2}$
0.0078125	$4.963 \cdot 10^{-3}$	$8.901 \cdot 10^{-6}$	$4.744 \cdot 10^{-3}$
0.00390625	$3.095 \cdot 10^{-3}$	$4.960 \cdot 10^{-6}$	$2.986 \cdot 10^{-3}$
0.001953125	$1.772 \cdot 10^{-3}$	$2.519 \cdot 10^{-6}$	$1.609 \cdot 10^{-3}$

Table 6.3: Relative error in mass loss for three phase model and/or two phase model.

[1] Starting with $\Gamma^{\gamma\alpha} = x_0$ and $\Gamma^{\alpha\theta}$ on the position the interface has at time of dissolution around 28.8 s.

Note that as the interface velocity of $\Gamma^{\alpha\theta}$ is a lot lower than that of $\Gamma^{\gamma\alpha}$, the time step is taken a lot bigger when austenite is dissolved. This gives overall a bigger mass lose during the two phase model.
Using this data we can find an approximation for the order of convergence using Richardson extrapolation. A CFL condition on the time step Δt is used, which makes Δt in order of the grid size h, meaning the first order accuracy of Euler backward is expected.
The results are shown in Table 6.4. We see that the three phase model is more accurate than the two phase model. This is (probably) because the mass gain over time is negative at the start of the three phase model, but positive later on (see Figure 6.4). Whereas the mass gain of the two phase model is always positive. This means mass is lost at the austenite/ferrite interface, but created at the ferrite/cementite interface. This effect results in a lower total mass gain, meaning the error is lower.

Start/end amount phases	approximated order
start: 3, end: 2 phases	0.72
start: 3, end: 3 phases	1.39
start: 2, end: 2 phases	0.78

Table 6.4: Order of convergence estimated by data in Table 6.3.

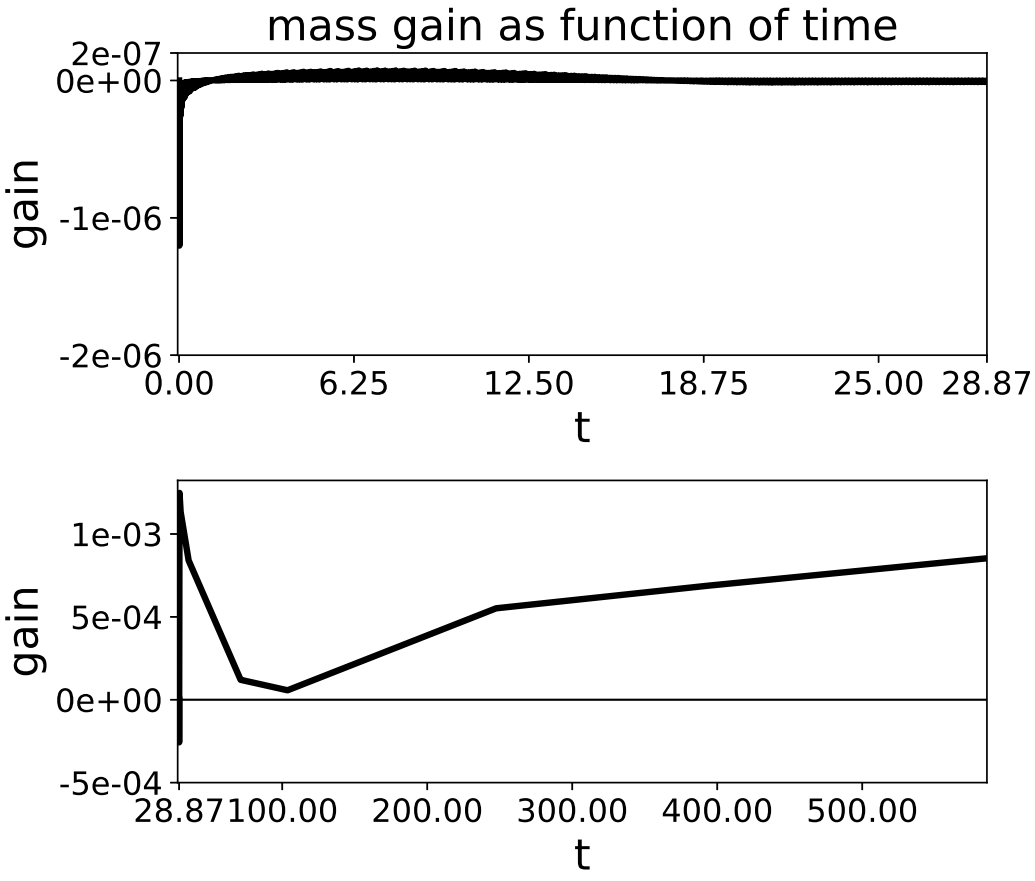

Figure 6.4: Mass gain over time for three (upper) -and two (lower) phases.

We also see that the accuracy over the whole simulation is lower than that of the three and two phase model individually. This means that in the transition of three to two phases an error is introduced. If we look at the mass gain over time of the

three phases individually, when the dissolution happens, we see that the mass of austenite, that was present just before dissolving, gets lost (see Figure 6.5). It is not added to the mass of ferrite or cementite. As the time steps get smaller for small grid sizes h, this effect should decrease when taking smaller grid sizes h, but the position of the interface $\Gamma^{\gamma\alpha}$ can still be relatively far from the outer boundary x_0 when the dissolution happens. Meaning this error does not always halves, when the grid size is halved. This explains the lower accuracy in the approximation of the total model.
There could also be an effect of the fact that there is a jump in the boundary condition as soon as austenite dissolves. At this moment ferrite comes in contact with the outer boundary $\partial\Omega$. On this boundary there is a homogeneous Neumann boundary condition, whereas before ferrite had a Dirichlet boundary condition on the $\Gamma^{\gamma\alpha}$ interface. More about this will follow in the next chapter.

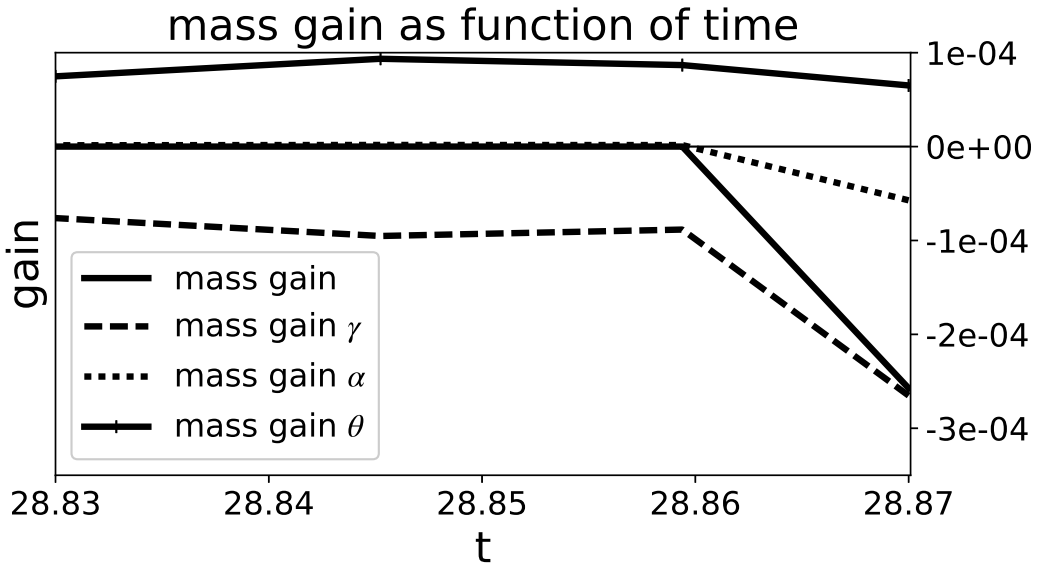

Figure 6.5: Mass gain over time close to dissolution at $t = 28.87$ s for the three phases individually and the total mass gain. The total mass loss at dissolution shows all austenite mass gets lost when dissolution happens.

6.3 Time integration

As noted in section 4.3 about time discretisation, Crank-Nicolson can experience oscillations in its solution. If we take the time step as

$$\Delta t = \min\left\{\Delta t_{\gamma\alpha}, \Delta t_{\alpha\theta}\right\},$$

where

$$\Delta t_{\gamma\alpha} = \min_{j=1,\ldots,N-1}\left\{\frac{h_j}{|v_n^{\gamma\alpha}|}\right\}, \Delta t_{\alpha\theta} = \min_{j=1,\ldots,N_\alpha-1}\left\{\frac{h_j^\alpha}{|v_n^{\alpha\theta}|}\right\},$$

like we use with the backward Euler, we see the oscillations in the ferrite concentration and interface velocity. See Figure 6.6 below.

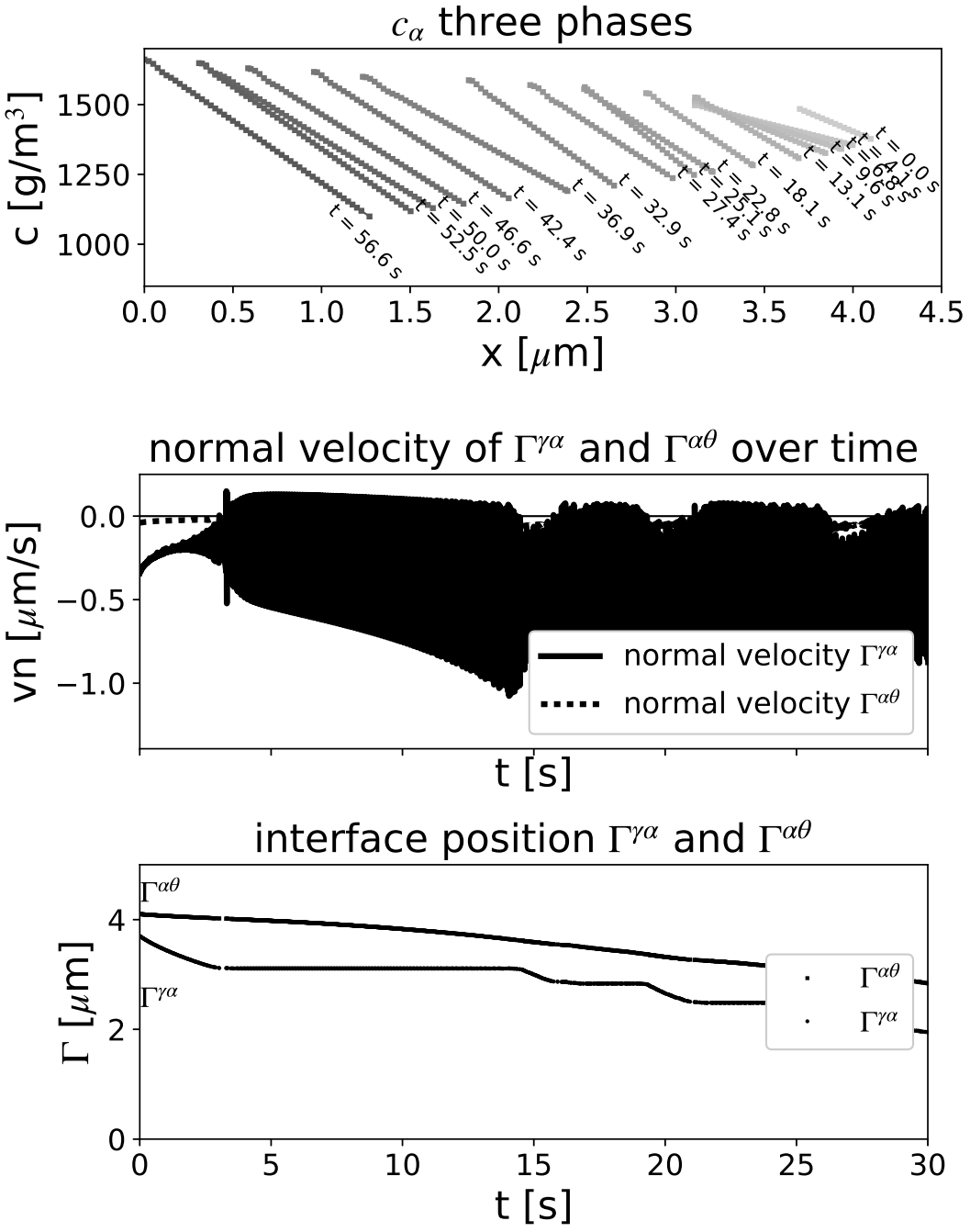

Figure 6.6: Oscillations near the $\Gamma^{\gamma\alpha}$ interface in the ferrite concentration (upper figure) and in the interface velocity/position of $\Gamma^{\gamma\alpha}$ (lower figures).

6.4 Cooling rates

To see the effect of the cooling rate $\frac{dT}{dt}$ we will show three simulations with the same model and parameters, only changing the cooling rate. We use $0.05, 0.4$ and 10 Ks^{-1}. See below for the interface velocity and position graphs and concentration curves with the different cooling rates.
For the low and medium cooling rates we see that the model is more diffusion controlled, as the concentration profile of austenite in the three phase model and ferrite in the two phase model are getting damped out. The concentration only changes because of the changing equilibrium concentration on the austenite/ferrite interface. For the high cooling rate we see that the interface velocity is much higher, which shows the austenite concentration does not have time to dampen out because of diffusion. The average velocity of the austenite/ferrite interface is high enough to dissolve the austenite before the temperature becomes constant.
The velocity for the high cooling rate is relatively lower at the time austenite dissolves than for the lower cooling rates. This is because the temperature is lower at the time of dissolution, here both the diffusion coefficients and reaction coefficients, which depends on the diffusion coefficient, are lower. Also for the lower cooling rates, both interface velocities are decreasing at a constant rate between 10 s and the time of dissolution. From the concentration profiles of c_γ, we see that in this time interval it is nearly constant. In the DDR/RDR comparison we saw that a proportionality factor $k_{0,\gamma\alpha} = 1$ gave a Dirichlet-like behaviour for the RDR model. We have that

$$v_n^{\gamma\alpha}(\mathbf{x},t) = -\frac{D_\alpha(\mathbf{x},t)}{c_{\alpha\gamma}^{\text{sol}}(\mathbf{x},t)}\frac{\partial c_\alpha}{\partial n}(\mathbf{x},t) + \frac{K^{\gamma\alpha}(\mathbf{x},t)}{c_{\alpha\gamma}^{\text{sol}}(\mathbf{x},t)}\left(c_{\gamma\alpha}^{\text{sol}}(\mathbf{x},t) - c_\gamma(\mathbf{x},t)\right), \quad \text{for } \mathbf{x} \in \Gamma^{\gamma\alpha}(t), t > t_0. \tag{6.3}$$

If $c_\gamma = c_{\gamma\alpha}^{\text{sol}}$ over Ω_γ, we know that the right hand side only depends on the diffusion coefficient D_α, the gradient of c_α and the equilibrium concentration of ferrite on the interface. So between $t = 10$ s and dissolution this should be a linear decreasing function.

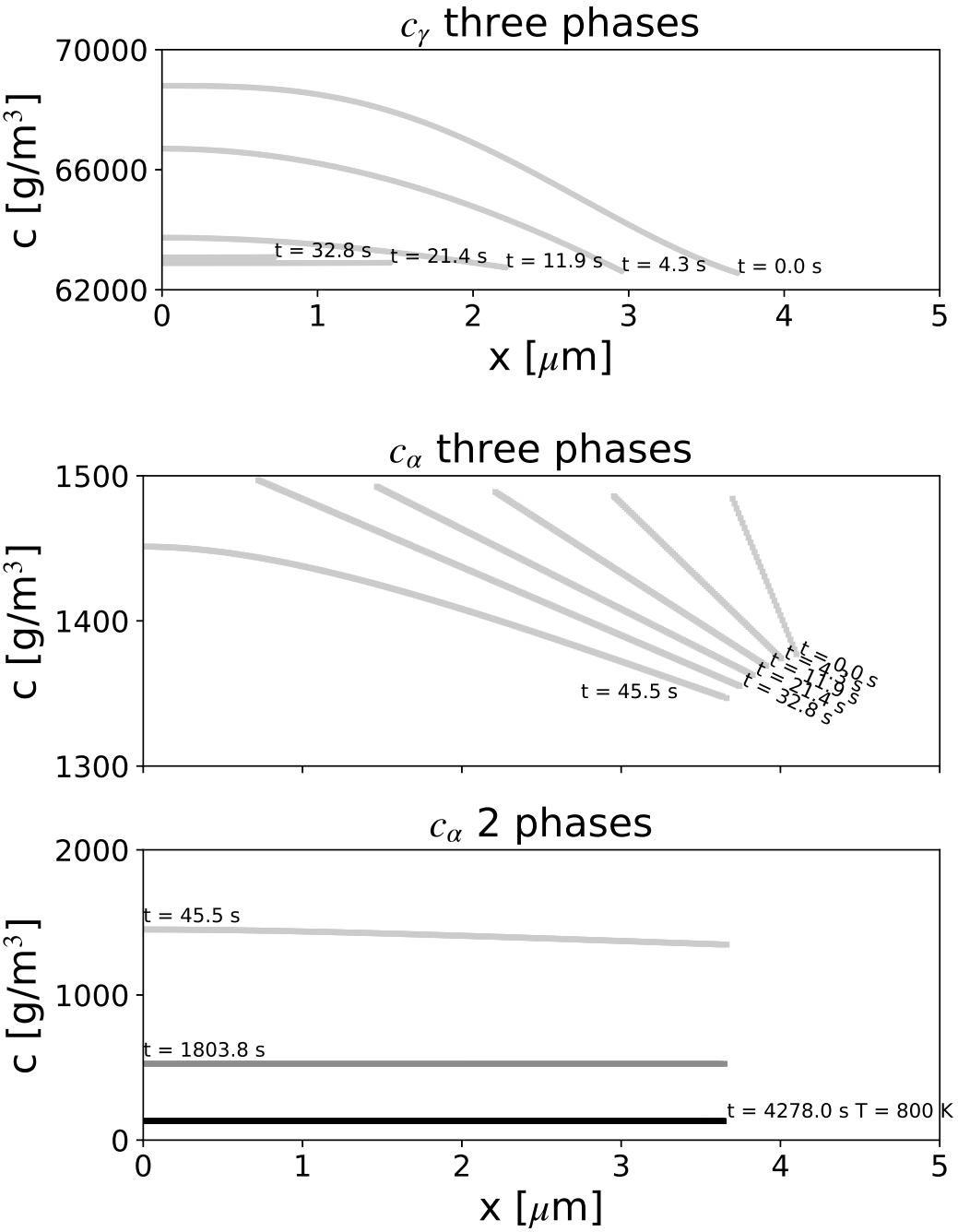

Figure 6.7: Concentration profiles for a low cooling rate 0.05 Ks^{-1}.

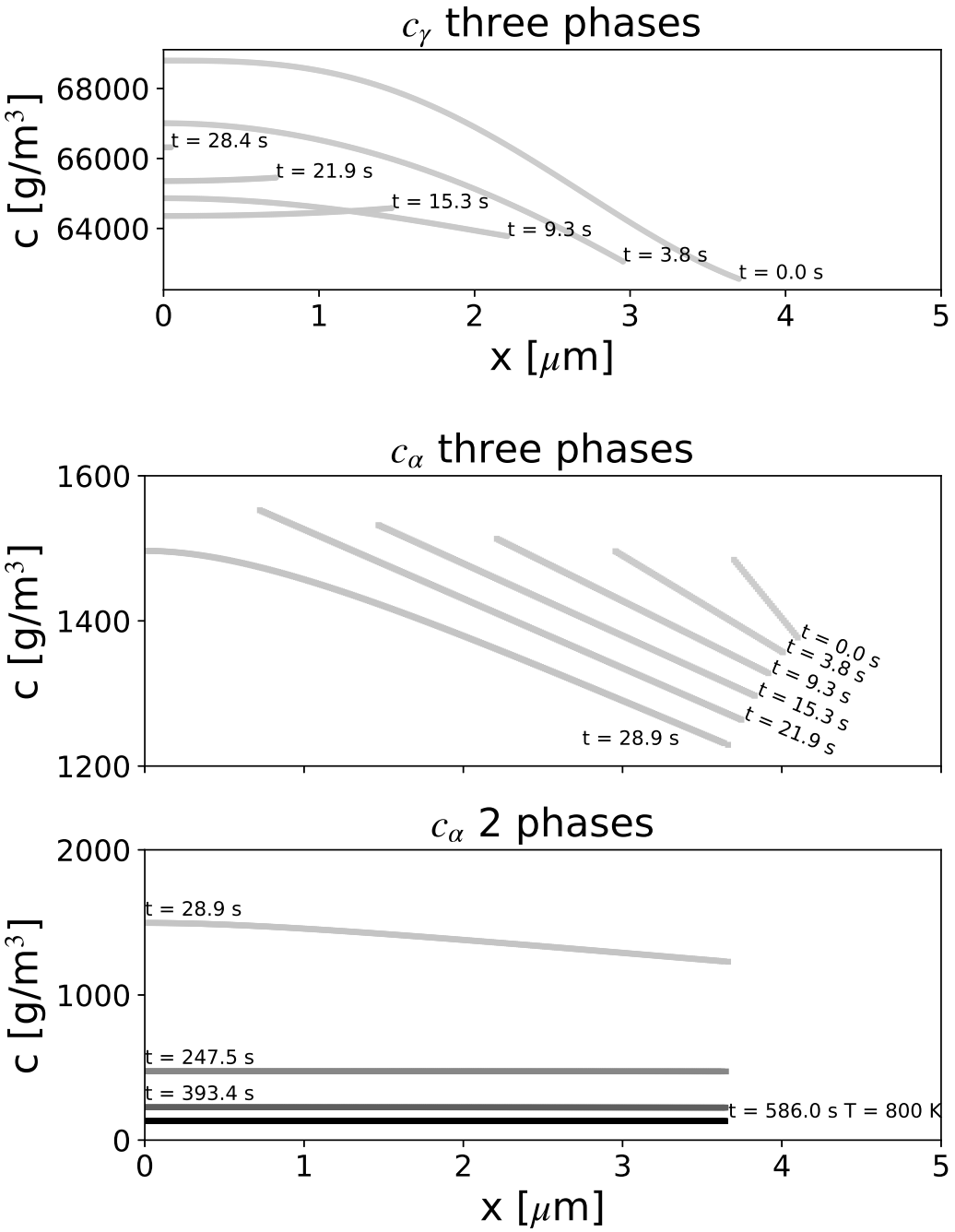

Figure 6.8: Concentration profiles for a medium cooling rate 0.4 Ks^{-1}.

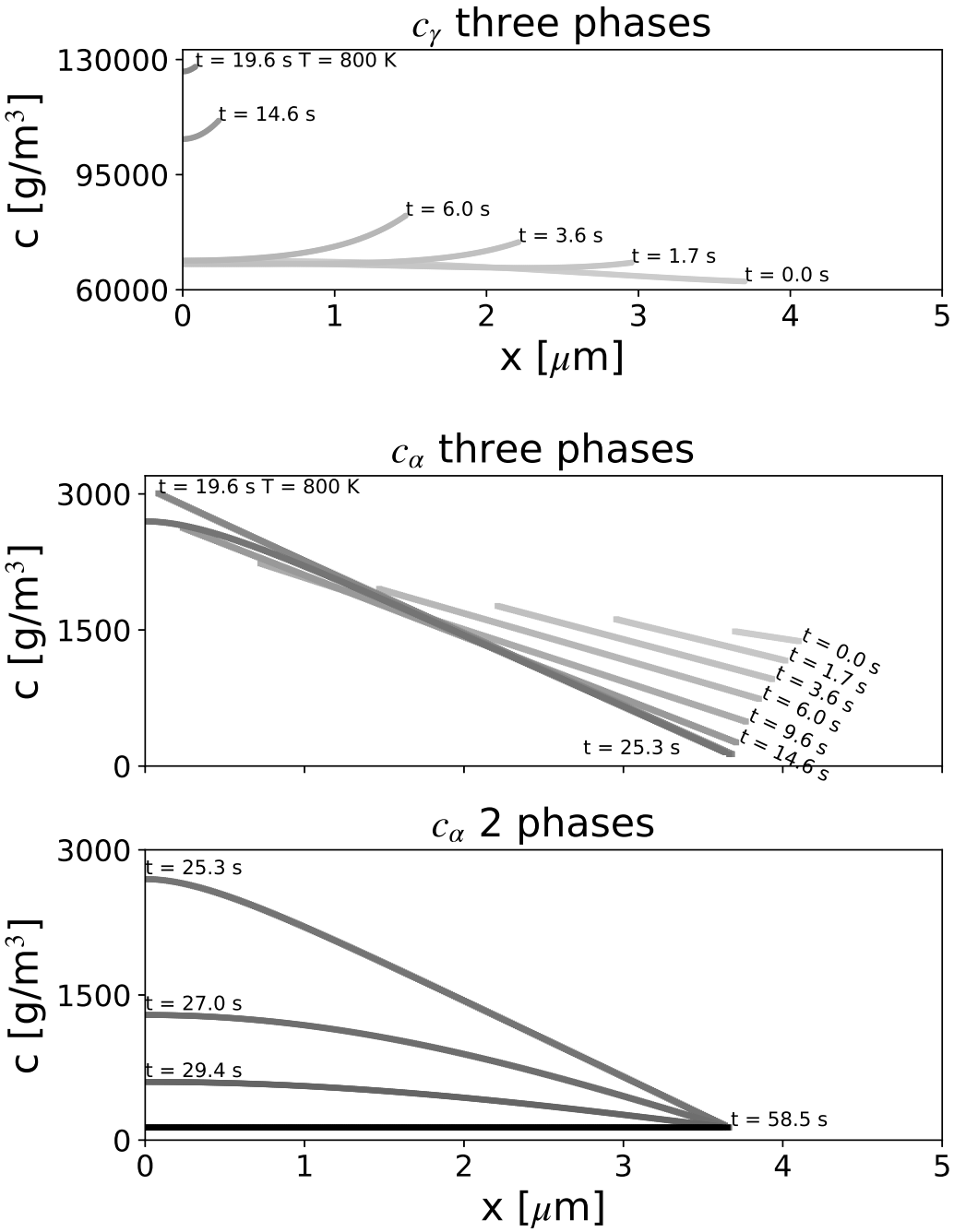

Figure 6.9: Concentration profiles for a high cooling rate 10 Ks^{-1}.

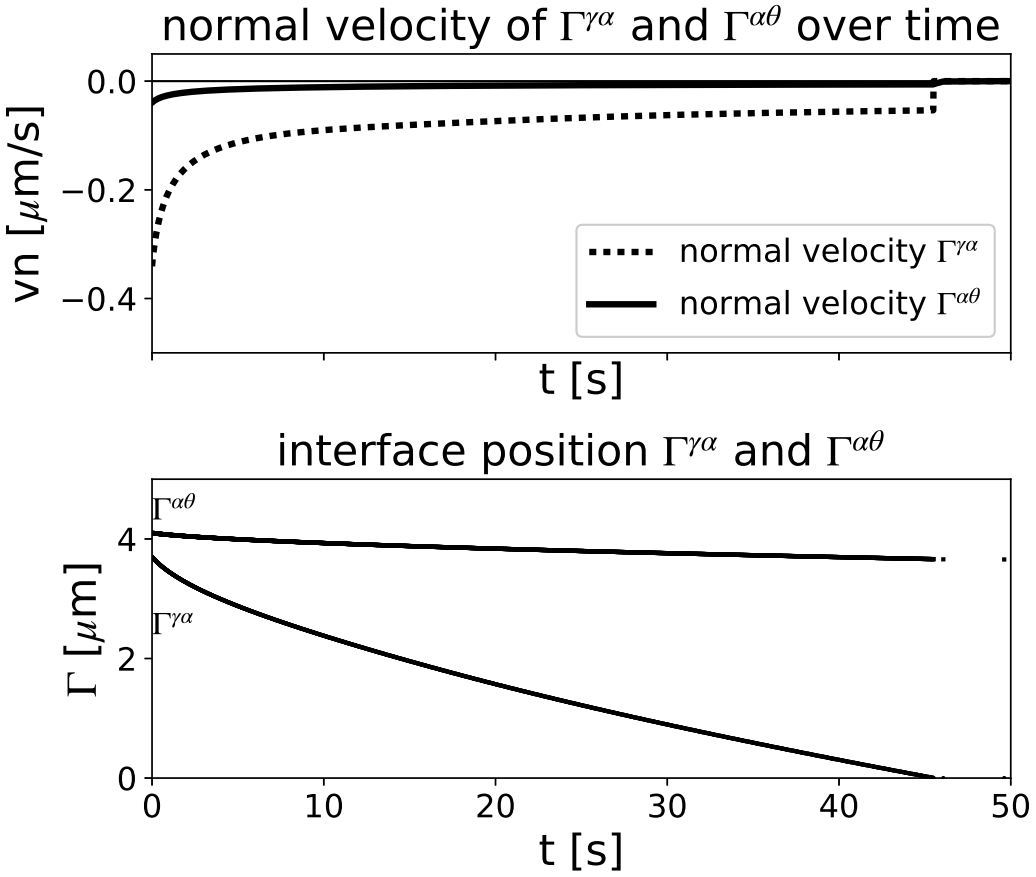

Figure 6.10: Interface velocity and position for a low cooling rate 0.05 Ks^{-1}.

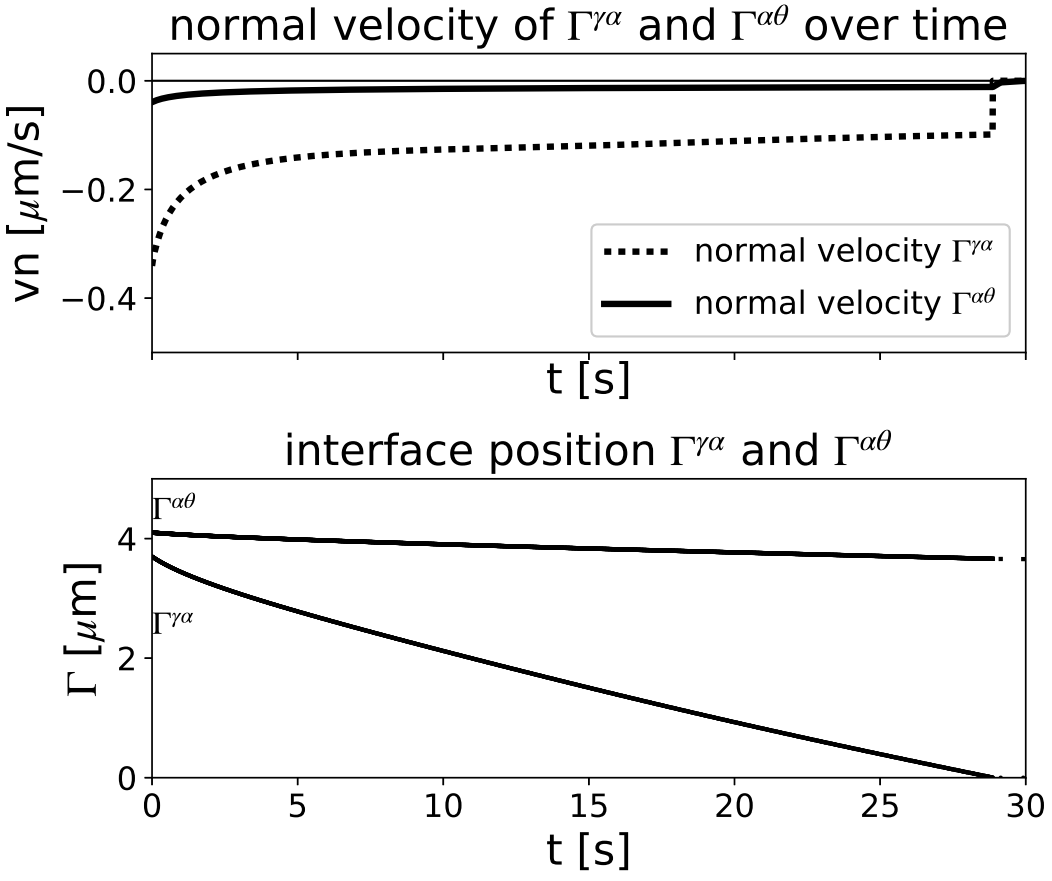

Figure 6.11: Interface velocity and position for a medium cooling rate 0.4 Ks^{-1}.

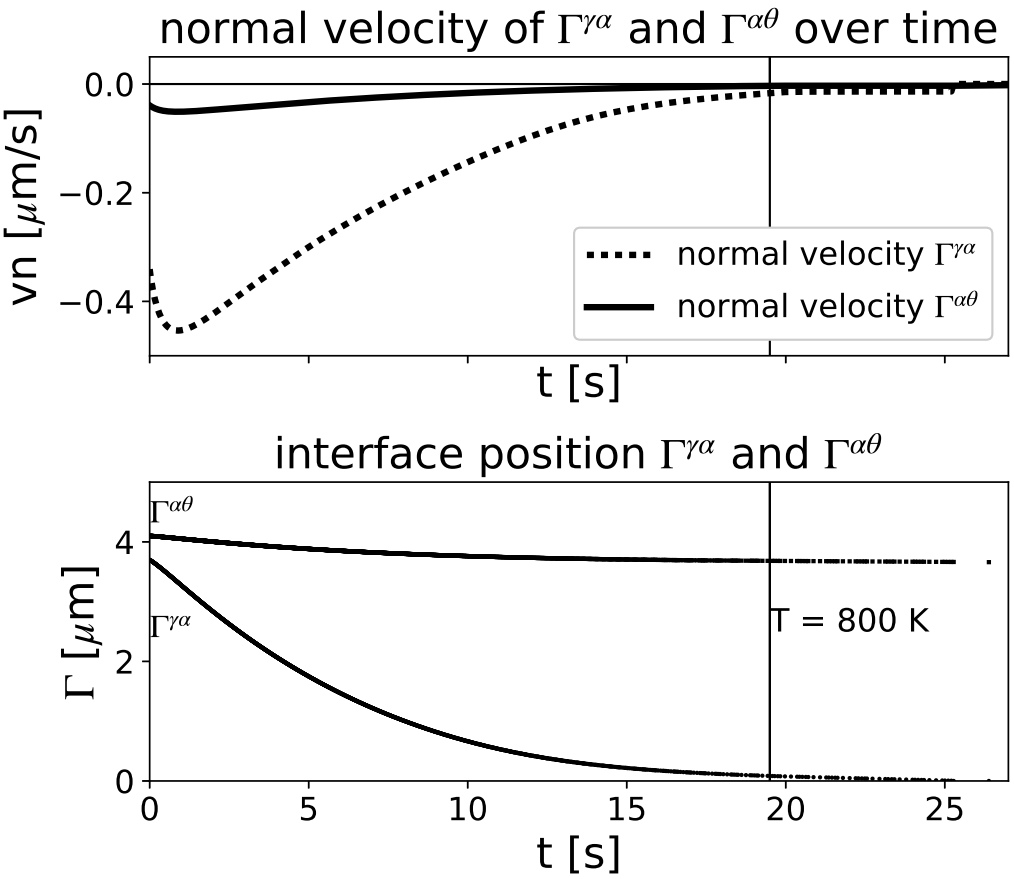

Figure 6.12: Interface velocity and position for a high cooling rate 10 Ks^{-1}.

Chapter 7

Discussion

This literature study is used as framework for a two dimensional Stefan problem describing austenite, ferrite and cementite phases in steel. Three options for the austenite/ferrite interface boundary condition were introduced, two different time discretisation methods were considered and three techniques have been looked at, in order to satisfy the dimensions in the FEM system. From the results of a 1D implementation given in the previous chapter we will decide which of these we choose or further investigate for the 2D model. Also some other results will be discussed which can be important or interesting for future work.

7.1 Results

We first looked at the three different boundary conditions for the austenite/ferrite interface. We showed that the RDR model is a more general case of the DDR model, which takes into account the mixed mode character of the matrix/matrix interface of austenite and ferrite. The movement of the interface is controlled by two physical effects, the interface reaction and diffusion. The DDR model only takes the diffusion controlled movement into consideration. This means it is assumed the interface reaction happens at a much faster rate, meaning the diffusion will control the model. This can be resembled in the RDR model by taking a higher value for the proportionality factor $k_{0,\gamma\alpha}$ in $K^{\gamma\alpha}$, which was also seen in the results.
The MDR model with a grain boundary condition on the austenite/ferrite interface is also a mixed mode character model. We found a relation between the MDR -and RDR model, which showed that the RDR has a similar Arrhenius relation for the mobility parameter, but it has a factor 2.2 difference in the proportionality factor χ

compared to the values found in the research of Mecozzi [5]. This can be explained by the fact that there are some differences between these two models. Her work is based on low-carbon steel, with carbon weight percentages between 0.05 % and 0.25 %, where ferrite nucleates and grows in austenite with no cementite present. The model is also performed for a two -and three dimensional model with a circular/spherical ferrite domain, which means there are more points of contact between the two phases. Comparing this to our one dimensional model, it could result in a higher proportionality factor, to have the same behaviour as a two -or three dimensional model.
All in all this means taking a reaction boundary condition on the austenite/ferrite interface is a reasonable, more general choice, which we will use for future work.

We saw that in order to solve the systems of equations for the concentration, a multiplication between the mass matrix M_k^{n+1} and the solution vector c_k^n was needed, where M_k^{n+1} is defined on the new mesh T_k^{n+1} and the solution c_k^n on the previous mesh T_k^n. Because of the way the mesh is discretized, the dimensions between these two objects are not always similar. Three techniques were given to extend the solution vector to comply to the new mesh. We called these techniques shift point, interpolate point and L2-projection. Shift point was seen to be the worst option, because mass was lost/gained on the interfaces. Both interpolate point and L2-projection are based on mass conservation, solving the problem the shift point technique has. Where interpolate point only considers the grid point that creates the mismatch, L2-projection moves all grid points from the old to the new mesh. This means a system of equations have to be created and solved, making it more time consuming. Interpolate point is a lot more simple as it only has to deal with the grid points that result in the mismatch. As interpolate point is just as easy as shift point and does not lead to mass creation/deletion on the interfaces, we will consider the interpolate point technique first in our future 2D model and afterwards implement the L2-projection technique.

In theory the Galerkin Finite Elements Method space discretisation should give second order convergence and first order convergence for the backward Euler time integration. In the results we saw that a first order convergence is barely attained for the whole model, for Δt in the order of h, but better results were found for only three -and two phases. This implies that there is an inaccuracy at the transition from three -to two phases when austenite dissolves. It turns out that the moment austenite dissolves, the mass of austenite that was present on the previous time step vanished. This problem occurs as the ferrite domain comes in contact with the

outer boundary, where a homogeneous Neumann is defined. Whereas before it was a Dirichlet boundary condition. The mass flux $c_\gamma v_n^{\gamma\alpha}$ gets lost in this time step. The jump in boundary conditions is also an open problem in the analysis of continuous moving boundary problems. We will have to tackle these problems in future work. More about this is shown below.

Using a second order time integration, like Crank-Nicolson, results in oscillations in the solution and interface velocities. These oscillations problems might possibly be solved with flux correction schemes like FCT (flux correction transport) [18] or algebraic flux correction [19]. However, as we have a working model, using backward Euler time integration, we avoid this. Another option would be using the θ-method. $\theta = \frac{1}{2}$ gives Crank-Nicolson, $\theta = 1$ gives backward Euler and $\theta = 0$ gives forward Euler. Taking a θ value somewhere in between will have, in theory, a linear order convergence, but close to second order and might not have oscillations. We might investigate this further for future work in order to get more accurate results in the two dimensional model.

When using different cooling rates $\frac{dT}{dt}$ from 995 K to 800 K, we can see several effects. For the higher cooling rate the concentration gradients are higher, as the mass gets pushed up. This is because of the higher interface velocity, meaning the interface movement controls the model, as is predicted in the work of Mecozzi [5]. The austenite concentration is able to attain higher values, because the temperature is lower before the austenite dissolves and for lower temperatures the equilibrium concentration for austenite is bigger. For lower cooling rates 0.05 Ks^{-1} and 0.4 Ks^{-1}, the mass does not get pushed up as hard as with the higher cooling rate 10 Ks^{-1} and diffusion dampens out the concentration, showing the model is diffusion controlled. As a result of the high cooling rate, the interface velocities are bigger. For the cooling rate of 10 Ks^{-1} it even is fast enough to make austenite dissolve before the end temperature is reached. In the steel production process, the steel normally gets cooled down almost instantly to a very low temperature, where the diffusion is so low that the whole carbon tranport process is stopped. This cooling is called quenching. From the different cooling rates we saw that a high cooling rate resulted in faster dissolution. So in the quenching process one could expect higher interface velocities during the time the temperature is still high enough, but goes to zero faster as the temperature drops faster.

7.2 Future work

- *Level-set 2D:* As shown in section 3.1 the level-set function for a 1D Stefan problem can be solved analytically and is not used in the algorithm whatsoever. However, keeping track of the interfaces is about the biggest problem in numerically approximating the two and three dimensional Stefan problem. In the continuation of this research a lot of research will be done regarding the evolution of the level-set functions.

- *Jump in boundary condition:* When determining the order of convergence of the algorithm, we found that the moment austenite dissolved and ferrite got in contact with the outer boundary, a numerical error was introduced, deteriorating the accuracy of the algorithm. This error was due to the loss of the austenite mass present just before dissolution. The problem lies in the fact that the model jumps from a Dirichlet condition to a homogeneous Neumann condition when the austenite dissolves and ferrite comes in contact with the outer boundary. The mass flux $v_n^{\gamma\alpha} c_\gamma$ seems to get lost during this time step. There is also another event that could introduce errors. When austenite dissolves and ferrite gets in contact with the outer boundary, the boundary condition for the ferrite/austenite-interface changes from Dirichlet to Neumann. This phenomenon is an open problem in the analysis of continuous moving boundary problems, so there is not much known yet about the implications this could have. The movement of the interfaces that are part of the model introduces non-linearty and together with this jump that could result to unpredictable behaviour.
  It should be possible to lessen the error that is introduced and improve global accuracy of the algorithm. In order to conserve the mass at the time step austenite dissolves, the no-flux condition could be set to an inhomogeneous Neumann condition, where the flux value is the flux $v_n^{\gamma\alpha} c_\gamma$ that should be there at dissolution. In order to tackle the jump in boundary condition one could apply a mass conserving L2-projection of the solution that suffices to the Neumann and the Dirichlet condition at the same time, as an intermediate time step on this jump. Another idea is to try to enforce the Dirichlet condition on the model together with the Neumann condition, with methods like the Langrange multiplier method.

- *Accuracy of time discretisation:* In order to improve global accuracy the θ-method could be used as an alternative for the backward Euler method. A full second order accuracy using $\theta = \frac{1}{2}$ results in oscillations, but a close-to

second order accuracy time discretisation with, for example $\theta = 0.55$, could be non-oscillatory for our model.

Bibliography

[1] D. den Ouden, *Mathematical Modelling of Nucleating and Growing Precipitates: Distributions and Interfaces*. PhD thesis, Delft University of Technology, 2015.

[2] F. Vermolen, E. Javierre, C. Vuik, L. Zhao, and S. van der Zwaag, "A three-dimensional model for patricle dissolution in binary alloys," *Computational Materials Science*, vol. 39, pp. 767–744, 2007.

[3] E. J. Perez, "Gibbs-thomson effects in phase transformations," *Scripta Materialia*, vol. 52, no. 8, pp. 709–712, 2005.

[4] W. Mullings and R. Sekerka, "Morphological stability of a particle growing by diffusion or heat flow," *Journal of Applied Physics*, vol. 34, no. 2, pp. 323–329, 1963.

[5] M. Mecozzi, "Phase field modelling of the austenite to ferrite transformation in steels," tech. rep., Delft University of Technology, 2006.

[6] C. Chen, *Cyclic Partial Phase Transformations In Low Alloyed Steels: Modeling and Experiments*. PhD thesis, Delft University of Technology, 2013.

[7] J. C. X. Zhang and S. Osher, "A multiple level set method for modeling grain boundary evolution of polycrystalline materials," *Interaction and Multiscale Mechanics*, vol. 1, no. 2, pp. 191–209, 2008.

[8] T. Illingworth and I. Golosnoy, "Numerical solutions of diffusion-controlled moving boundary problems which conserve solute," *Journal of Computational Physics*, 2005.

[9] Cenna, "Phase field order parameter." `https://upload.wikimedia.org/wikipedia/commons/e/e7/Phase_field_order_parameter.jpg`, 2008.

[10] R. Qin and H. Bhadeshia, "Lecture 15: Phase field modelling," *Materials Science & Metallurgy*, vol. 26, no. 7, 2010.

[11] C. Gauss, "Gauss quadrature formula." http://www.encyclopediaofmath.org/index.php?title=Gauss_quadrature_formula&oldid=11718, 2011.

[12] J. Thomas, "Numerical partial differential equations: Finite difference methods," *Springer-Verlag*, vol. 22, p. 386, 1995.

[13] R. LeVeque, *Finite Difference Methods for Ordinary and Partial Differential Equations: Steady-State and Time-Dependent Problems*. Cambridge University Press, 2007.

[14] S. Arrhenius, "Über die dissociationswärme und den einfluss der temperatur auf den dissociationsgrad der elektrolyte," *Zeitschrift fur Physikalische Chemie*, vol. 4, 1889.

[15] M. Wieser, "Atomic weights of the elements," *Pure and Applied Chemistry*, vol. 78, no. 11, p. 20512066, 2005.

[16] U. N. I. of Standards and Technology, "Codata value: molar gas constant." http://physics.nist.gov/cgi-bin/cuu/Value?r, 2015.

[17] M. Onink, C. Brakrnan, F. Tichelaar, E. Mittemeijer, and S. van der Zwaag, "The lattice parameters of austenite and ferrite in fec alloys as functions of carbon concentration and temperature," *Scripta Metallurgica*, vol. 29, pp. 1011–1016, 1993.

[18] M. Möller, D. Kuzmin, and S. Turek, *Implicit flux-corrected transport algorithm for finite element simulation of the compressible Euler equations*. Springer Berlin Heidelberg, 2004.

[19] M. M. D. Kuzmin, *Algebraic Flux Correction I. Scalar Conservation Laws*. Springer Berlin Heidelberg, 2005.